



Contamination in mafic mineral-rich calc-alkaline granites: a geochemical and Sr-Nd isotope study of the Neoproterozoic Piedade Granite, SE Brazil

RENATO J. LEITE, VALDECIR A. JANASI and LUCELENE MARTINS

Instituto de Geociências, Universidade de São Paulo
Rua do Lago, 562, 05508-080 São Paulo, SP, Brasil

*Manuscript received on December 3, 2004; accepted for publication on November 22, 2005;
presented by MIGUEL A.S. BASEI*

ABSTRACT

The Piedade Granite (~600 Ma) was emplaced shortly after the main phase of granite magmatism in the Agudos Grandes batholith, Apiaí-Guaxupé Terrane, SE Brazil. Its main units are: mafic mineral-rich porphyritic granites forming the border (peraluminous muscovite-biotite granodiorite-monzogranite MBmg unit) and core (metaluminous titanite-bearing biotite monzogranite BmgT unit) and felsic pink inequigranular granite (Bmg unit) between them. Bmg has high La_N/Yb_N (up to 100), Th/U (>10) and low Rb, Nb and Ta, and can be a crustal melt derived from deep-seated sources with residual garnet and biotite. The core BmgT unit derived from oxidized magmas with high Mg# (~45), Ba and Sr, fractionated REE patterns ($La_N/Yb_N=45$), $^{87}Sr/^{86}Sr(t) \sim 0.710$, $\epsilon Nd(t) \sim -12$ to -14 , interpreted as being high-K calc-alkaline magmas contaminated with metasedimentary rocks that had upper-crust signature (high U, Cs, Ta). The mafic-rich peraluminous granites show a more evolved isotope signature ($^{87}Sr/^{86}Sr(t) = 0.713-0.714$; $\epsilon Nd(t) = -14$ to -16), similar to Bmg, and Mg# and incompatible trace-element concentrations intermediate between Bmg and BmgT. A model is presented in which MBmg is envisaged as the product of contamination between a mafic mineral-rich magma consanguineous with BmgT and pure crustal melts akin to Bmg.

Key words: granite, calc-alkaline, peraluminous, magma contamination, Sr-Nd isotope geochemistry.

INTRODUCTION

The origin of mafic mineral-rich peraluminous granites has been much debated since Chappell and White's (1974) proposal that the S-type granites from the Lachlan Fold Belt (LFB) in Australia owe their unfractionated character to the presence of significant amounts of restitic material into a low-temperature, crust-derived minimum melt. In recent years, several lines of evidence, such as experimental (Patiño-Douce 1999), isotopic (Keay et

al. 1997) and the study of enclaves (Barbarin 1999) have indicated that a non-metasedimentary component is probably present in many of these granites, including some LFB S-types (Elburg 1996, Collins and Hobbs 2001). The nature of this component may be diverse, but most authors admit it as ultimately mantle-derived. Incorporation of an important amount of metasedimentary rock-derived material is however required for the generation of the mafic peraluminous granites, because other processes that can increase the alumina saturation index (ASI) in granites such as crystal fractiona-

Correspondence to: Valdecir de Assis Janasi
E-mail: vajanasi@usp.br

tion and hydrothermal alteration will typically generate felsic rocks (e.g., Zen 1986). Sites where interaction between a mantle-derived magma and metasedimentary rocks may be effective include: (1) the lower crust, where processes such as MASH (melting, assimilation, storage and homogenization) seem to be common and could explain the generation of calc-alkaline magmas in active continental margins (Hildreth and Moorbath 1988), (2) the pathway followed by originally non-peraluminous magmas through the crust or (3) the sites of final emplacement of these magmas, where metasedimentary country rocks may be digested.

The 600 Ma Piedade granite in SE Brazil is a zoned elliptical pluton with an extensive border unit with higher color index (CI = 14–8 porphyritic muscovite-biotite granite-granodiorite, a contrasted core unit of dominantly metaluminous porphyritic titanite-biotite granite (CI ~ 8), with an intervening unit of lighter (CI = 5–6) biotite-only pink inequigranular monzogranite (Fig. 2). The pluton is marginal to, and slightly younger than, the voluminous 610–615 Ma porphyritic hornblende-biotite granites (CI = 14–8) that make up the bulk of the Agudos Grandes batholith (Janasi et al. 2001), a major tectonic unit of the Neoproterozoic Apiaí-Guaxupé Terrane in the Mantiqueira Province, SE Brazil. Detailed mapping of the Piedade granite, together with mineral (L. Martins, unpublished data) and rock chemistry (R.J. Leite, unpublished data), as well as Sr-Nd isotope geochemistry shed light on the mechanisms responsible for its compositional variation, including the peculiar more mafic peraluminous unit.

GEOLOGICAL SETTING

GEOLOGICAL EVOLUTION OF SE BRAZIL IN THE NEOPROTEROZOIC

Geological evolution of SE Brazil in the Neoproterozoic was complex, and involved at least two major continental plates: the southernmost São Francisco-Congo craton and the “Paranapanema” craton (Fig. 1). The latter is presently covered by Phanero-

zoic sedimentary rocks and volcanic rocks of the Paraná Basin, and possibly corresponds to the northernmost portion of the Rio de La Plata craton (Fig. 1; cf. Campos Neto 2000). The Neoproterozoic fold belts surrounding these cratons contain a number of distinct geological domains, differently described as “terrane”, “microplates” etc, many of which have uncertain paleogeographical relationships with each other and/or with the cratonic masses. In SE Brazil, the Paranapanema craton is surrounded in the NE by the Socorro-Guaxupé Nappe (SGN; the southernmost part of the NW-trending Brasília Belt) and in the SE by the NE-trending Apiaí-São Roque Domain (ASRD in Fig. 1). The SGN and ASRD are magmatic arc terranes thought to have developed at the margin of the Paranapanema craton, and are referred to as the Apiaí-Guaxupé Terrane (Campos Neto 2000; Fig. 1). The Brasília Belt verges towards the São Francisco craton, and includes extensive Neoproterozoic sedimentary basins (Piuzana et al. 2003) and magmatic arcs, which evolved from intra-oceanic at ~800 Ma to intra-continental at ~625 Ma (Pimentel et al. 1997, Campos Neto 2000). Most of the metasedimentary sequences within the ASRD were deposited in the Mesoproterozoic (e.g., Basei et al. 2003; see also Juliani et al. 2000) and could already be part of the Paranapanema plate prior to the Neoproterozoic orogenies (e.g., Campos Neto 2000). Neoproterozoic basins seem to be restricted and in part of continental origin in ASRD; nevertheless, early metavolcanosedimentary sequences with pillow-lava basalt were described as ophiolite sequences (Tassinari et al. 2001), and extensive high-K calc-alkaline granite batholiths were formed between 625 and 600 Ma (e.g., Gimenez Filho et al. 2000, Janasi et al. 2001, Prazeres Filho et al. 2003).

The NE-trending terranes located E-SE of the Apiaí-São Roque Domain (of which Embu, Juiz de Fora and Coastal are shown in Fig. 2), usually referred to as the Central Ribeira Belt, were accreted to the growing continental mass formed by the amalgamation of the São Francisco and Paranapanema cratons during the later Rio Doce (~590–565 Ma)

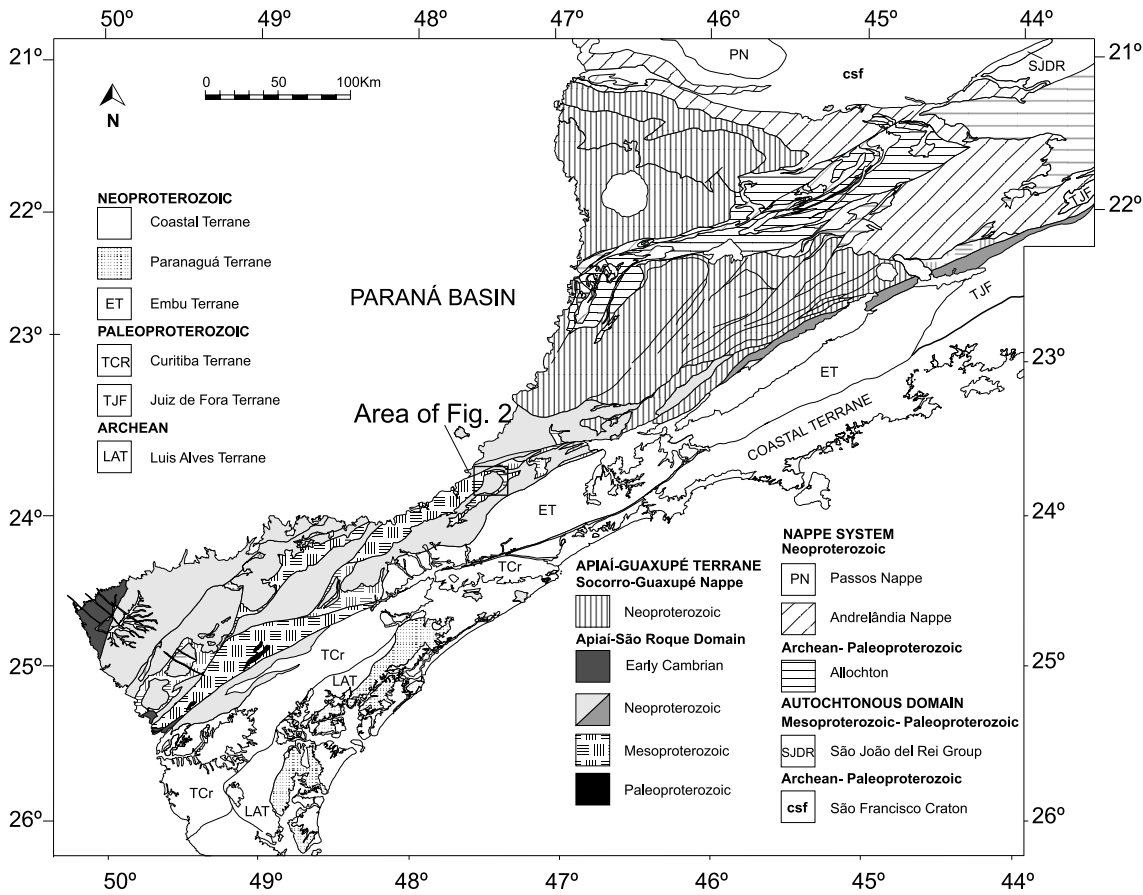


Fig. 1 – Tectonic map of SE Brazil showing the Apiaí-Guaxupé Terrane and neighboring tectonic units (modified from Heilbron et al. 2004).

and Cabo Frio (~530–520 Ma) orogenies (Heilbron and Machado 2003). During the Rio Doce orogeny, the Apiaí-Guaxupé Terrane behaved as a stable area and was affected by transcurrent faults and intruded by the epizonal post-orogenic granites of the Itu Province (Vlach et al. 1990).

THE AGUDOS GRANDES BATHOLITH

Large portions of the Apiaí-Guaxupé Terrane are occupied by elongated batholiths dominated by high-K calc-alkaline porphyritic hornblende-biotite granites. These are considered as “syn-orogenic” on the basis of structural relationships; Spanner and Kruhl (2002) showed that they intruded along WSW-directed low-angle thrust planes developing a magmatic foliation that is parallel to solid-state fabrics

within the country rocks. The most reliable U-Pb dates point towards a peak of granite production in the 615–605 Ma period (Gimenez Filho et al. 2000, Janasi et al. 2001, R.J. Leite, unpublished data); however, Prazeres Filho et al. 2003 suggest that the main “syn-orogenic” magmatism could have already started by ~ 625 Ma.

The Agudos Grandes Batholith (AGB) crops out within the easternmost block attributed to the ASRD. To the east it is limited by the Embu Terrane, which is already considered by Campos Neto (2000) as part of the Central Ribeira Belt. The AGB is elongated with a major axis running NE-SW for ~240 km and a width of 20–70 km, and intrudes the Mesoproterozoic Perau Group (Campanha and Sadowski 1999), a volcano-sedimentary sequence

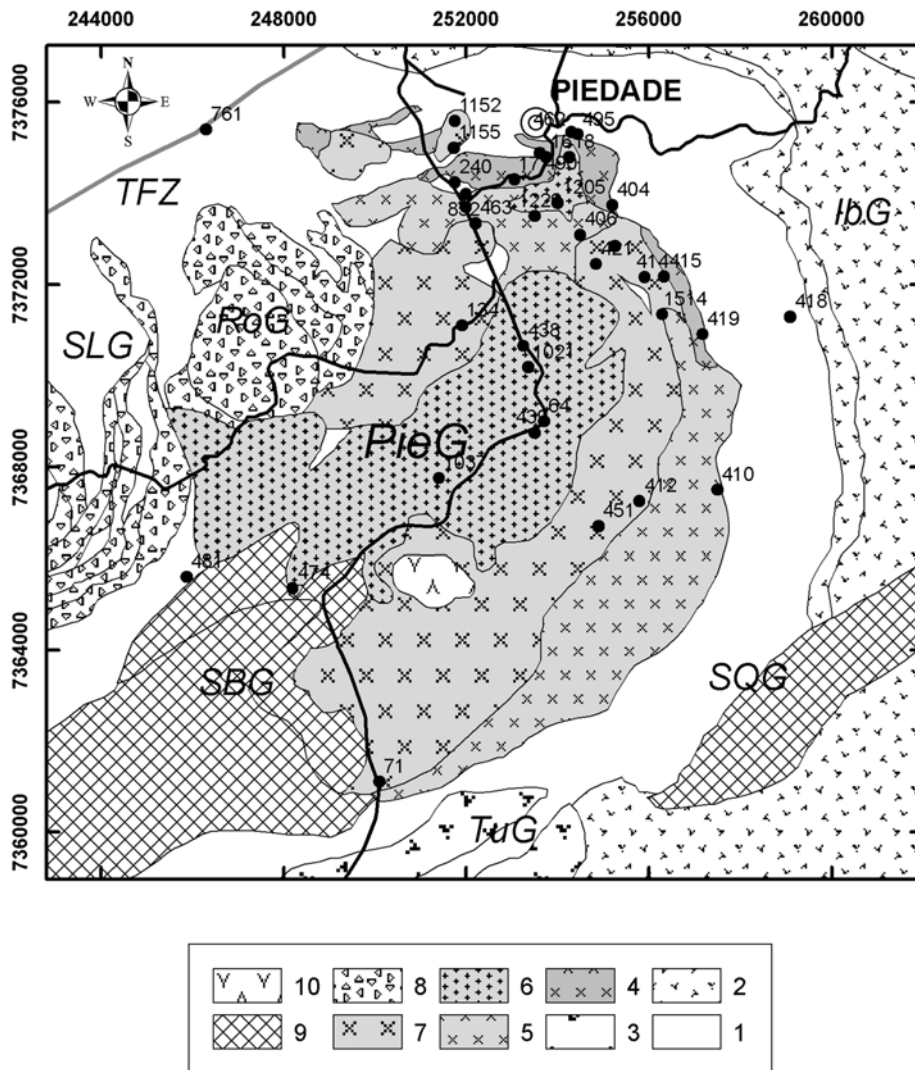


Fig. 2 – Geological sketch map of the Piedade granite and neighbor plutonic occurrences (modified and simplified from R.J. Leite unpublished data). Legend: 1= Pilar do Sul Metamorphic Complex; 2= Ibiúna syn-orogenic Granite; 3= Turvo syn-orogenic Granite; 4 to 7= Piedade late-orogenic Granite (4= porphyritic Ms-Bt granodiorite MBgd, 5= porphyritic Ms-Bt monzogranite MBmg, 6= porphyritic Bt granite BmgT, 7= inequigranular Bt granite Bmg); 8= other late-orogenic granites; 9= post-orogenic granites; 10= Cretaceous alkaline rocks. Abbreviations: Ib.G= Ibiúna Granite; PieG= Piedade Granite; RoG= Roseira Granite; SBG= Serra da Batéia Granite; SLG= Serra dos Lopes Granite; TFZ= Taxaquara Fault Zone; TuG= Turvo Granite. Numbers refer to location of samples with chemical analysis. Longitude, latitude: UTM E and N, in meters.

metamorphosed to low-grade, but grading quickly to high-grade in the easternmost limits of the batholith.

A wide diversity of granite types was already recognized in early mapping studies of the AGB

(Hasui et al. 1969, Y. Hasui, unpublished data). Mapping in a more detailed scale led to the recognition of several granite bodies with different ages and chemical affinities (D.P. Stein, unpublished data, Godoy et al. 1999). Janasi et al. (1990) dis-

tinguished three main associations in the eastern half of the batholith, emplaced during the syn-, late- and post-orogenic stages. This subdivision has been later supported by U-Pb zircon and monazite dating, which indicated ages of 610 ± 2 Ma for the syn-orogenic high-K calc-alkaline metaluminous type that forms the Ibiúna Granite (the more voluminous rock type), and also for the small peraluminous Turvo leucogranite, 600–605 Ma for the late-orogenic Piedade granite, and 565 ± 8 Ma for the post-orogenic Serra da Batéia granite (Janasi et al. 2001).

GEOLOGY OF THE PIEDADE GRANITE

The ~ 100 km² Piedade Granite is an elliptical N45E trending zoned pluton. It intrudes migmatized schists and gneisses to the east, and was intruded, in its western sector, by the younger Roseira and Serra da Batéia granites (Fig. 2). The pluton has a complex zoning, with more mafic porphyritic units at the border and core, and an intermediate more felsic unit between them.

The border facies (collectively referred to as MBmg) occur is a ring-shaped arrangement of narrow elongated bodies of porphyritic muscovite-bearing biotite granodiorite to monzogranite (CI = 11–14) followed inwards by a lighter monzogranite (CI = 8–10) as two larger discontinuous bodies. Pink alkali feldspar megacrysts (1–2 cm long) usually define a magmatic foliation. Oriented recrystallization of quartz and micas in the groundmass evidence recrystallization in the solid state. In several places, the border units intrude the host mica-schists as concordant sheets, sometimes enclosing small xenoliths. A 601 ± 2 Ma U-Pb monazite age was obtained for the MBmg unit (Janasi et al. 2001). In the northern portion of the pluton, a white-alkali-feldspar facies yielding a distinctive very low magnetic susceptibility predominates. In some outcrops, boulders of this variety alternate at a meter scale with the pink-alkali-feldspar facies of higher magnetic susceptibility. This situation suggests that the latter were locally produced by oxidation of the

first (cf. L. Martins, unpublished data).

The intermediate unit consists of discontinuous bodies of biotite monzogranite (Bmg) and is locally intrusive into the border porphyritic granites. These rocks are the least foliated and the most felsic in the Piedade granite. The predominant facies is inequigranular medium to coarse-grained (CI = 6–7), but locally a coarser facies with lower CI (4–5) occurs. A U-Pb discordia obtained from a few inheritance-free zircon and monazite crystals indicated a 605 ± 7 Ma age (Janasi et al. 2001).

The core of the pluton consists of a weakly foliated titanite-bearing porphyritic biotite monzogranite unit (BmgT, CI = 7–11), forming an elongated NE-SW shaped body. Biotite in this unit is coarser, a distinctive field aspect that aids in its mapping. Janasi et al. (2001) obtained a U-Pb zircon discordia with upper intercept at 604 ± 8 Ma for this unit, which is intruded by the younger ~ 565 Ma Serra da Batéia Syenogranite (Fig. 2).

Enclaves are abundant in both the border and core porphyritic units. The more common enclave type found in the border peraluminous MBmg unit are 1–2 cm biotite clots that grade into the granite host. Elliptical decimeter-sized microgranular enclaves of intermediate (tonalite to melagranite) composition are much rarer, and occur mainly along the northern portion of the pluton. Xenoliths clearly derived from the country rock (mica-schists and calc-silicate rock) may be abundant in contact zones. Lens-shaped bodies (decimeter- to a few meters-wide) of foliated medium-grained hornblende-biotite granodiorite (CI = 22–27), locally with 1–2 cm hornblende clots, occur in a few localities.

The enclaves in BmgT are centimeter-sized elliptical bodies of medium-grained biotite-rich tonalite and granodiorite (CI ~ 30). The smaller bodies grade into biotite-rich *schlieren* or clot-rich domains. The Bmg unit is usually poor in enclaves, but one outcrop in the north-central portion of the pluton shows a cluster of decimeter-sized elliptical microgranular enclaves separated from each other by thin granite veins that was apparently derived from the disruption of mafic dikes.

PETROGRAPHY AND REDOX CONDITIONS

The results from modal analyses of granites and enclaves of the Piedade pluton are presented in Figure 3. Monzogranite compositions are largely predominant, with a few samples from MBmg plotting in the granodiorite and half of the samples from Bmg in the syenogranite field.

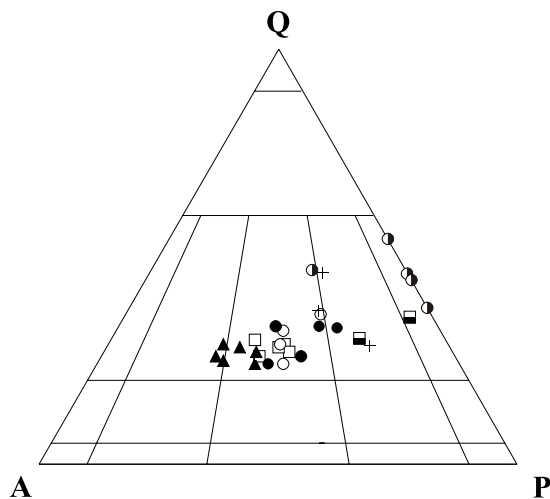


Fig. 3 – Modes of the Piedade granite expressed in terms of QAP and Q and P versus CI (color index). Symbols: closed circles, mafic MBmg; open circles, felsic MBmg; half-filled circles, enclaves in MBmg; open squares, BmgT; half-filled squares, enclaves in BmgT; closed triangles, Bmg; crosses, granodioritic lenses.

The enclaves are distinguished by their high color indices (25–40) and, in some cases, high quartz contents (cf. tonalite enclaves in the MBmg unit).

Plagioclase is weakly zoned, and is typically a calcic oligoclase; a few more mafic samples from MBmg show andesine (An_{33–35}). Alkali feldspar megacrysts are perthitic microcline rich in plagioclase and biotite inclusions. Matrix quartz and alkali feldspar are usually interstitial.

Biotite is pleochroic in shades of brown, except in MBmg samples with white alkali feldspar, where it is foxy-red. Primary muscovite, recognized by its euhedral shape, may reach up to 4% in volume in some MBmg samples.

Monazite is an important accessory mineral in

MBmg, especially in the more mafic samples. Titanite and allanite are abundant in the core BmgT unit, which is monazite-free. Ti-free magnetite is the main opaque mineral in the latter unit; only a few traces of relict hematite-rich ilmenite are found within titanite crystals. L. Martins (unpublished data) based on mineral chemistry estimated strongly oxidizing conditions ($\Delta\text{NNO} \geq +2$) during the crystallization of the core unit. Magnetite and ferri-ilmenite are the usual oxide minerals of the border unit, while hematite-poor ilmenite is the sole Fe-Ti oxide in the variety with white alkali feldspar and red biotite, which crystallized under reducing conditions (close to QFM; L. Martins, unpublished data).

The enclave mineralogy usually follows that of the country granite: enclaves within MBmg are usually muscovite-bearing, while those from BmgT are rich in titanite and allanite. An important exception is the hornblende-biotite granodiorite found as lenses within MBmg. This rock has up to 3% of magmatic epidote (euhedral crystals, many with allanite cores; cf. Schmidt and Thompson 1996, Sial et al. 1999), and up to 1% titanite. Magnetite is absent, a common feature in rocks with magmatic epidote.

ELEMENTAL GEOCHEMISTRY

ANALYTICAL PROCEDURES

Major and some trace elements (Ba, La, Sr, V, Y and Zr) were analyzed at the ICP-OES Laboratory, Instituto de Geociências, Universidade de São Paulo, Brazil. Samples powdered to < 200 mesh in an agate mill were taken into solution by alkaline fusion using a mixture of 0.25 g rock powder and 0.75 g flux (lithium tetra and metaborate). HNO₃ 0.2 N solutions diluted to 1:1000 were analyzed in an ARL-3410 sequential spectrometer; complete descriptions of these procedures can be found in Janasi et al. (1995).

Analyses of a set of trace elements (REE, Th, U, Cs, Hf, Ta, Cr, and Sc) were obtained in some samples by instrumental neutron activation (INAA) at Activation Laboratories (ACTLABS, Canada); in

other samples, the same elements and some others (Nb, Y, Ni, Co, Zr, W, Sn) were analyzed by ICP-MS at the Plasma Analytical Laboratory, Kansas University, USA. Whenever one element was analyzed by more than one technique, the result obtained by ICP-MS was chosen, as the detection limits are lower, and the REE patterns are more complete.

MAJOR, MINOR AND MAIN TRACE ELEMENTS

Chemical data from granites and their enclaves from the Piedade pluton are presented in Table I and in conventional variation diagrams in Figure 5. The granitic rocks span a relatively wide silica range (64 to 73 wt% SiO₂), while the enclaves are more basic, with 56–67 wt% SiO₂.

Diagrams using the SiO₂ and Al₂O₃ contents and indices such A/CNK (molecular Al₂O₃ / (CaO + Na₂O + K₂O)) and Mg# (molecular MgO / (MgO + FeO_T)) conveniently discriminate the different studied granite units. Samples from the BmgT unit clearly differ from the other granites by their higher Mg# (Figure 4), which is mostly a reflection of their higher MgO contents (Figure 5). Unit Bmg, discriminated in the field by its lower mafic content, seems to follow the major-element evolution tendencies of the muscovite-bearing MBmg unit (cf. Al₂O₃, Mg# × SiO₂ diagrams, Figures 4 and 5). We notice, however, that no clear negative correlation between Mg# and SiO₂ is observed within the MBmg trend (Fig. 4), and thus the lower average Mg# shown by Bmg (34.3 *versus* 38.1 in MBmg), which is similar to those of other felsic late-orogenic granites in the AGB (R.J. Leite, unpublished data) may not be the result of simple magma differentiation.

Apart from the above-mentioned chemical discriminants, there is a remarkable compositional overlapping between the two main evolutionary trends identified in the Piedade pluton (Figure 5). BmgT is slightly enriched in Ti, Ba and Sr, but at SiO₂ > 70 wt% these elements contents seem to be similar, and it is difficult to associate the Bmg unit to any of the two lineages. More scatter is commonly

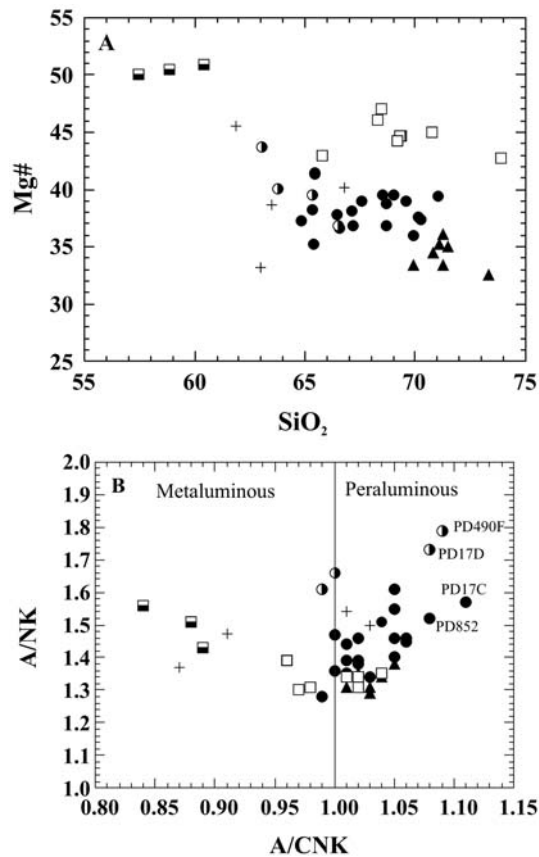


Fig. 4 – Behavior of the different facies of the Piedade granite in terms of major-element discrimination indices: (a) Mg# x SiO₂ and (b) ASI x A/NK. Symbols: closed circles, mafic and felsic MBmg; half-filled circles, enclaves in MBmg; open squares, BmgT; half-filled squares, enclaves in BmgT; closed triangles, Bmg; crosses, granodioritic lenses.

observed in the MBmg unit, which can reflect processes acting at a local scale or the existence of as yet unrecognized different lineages. Examples are samples 379 and 490b: the first one shows high K/Na and is anomalously enriched in P, Zr and Sr, and the second shows low K/Na and is Sr-rich (Figure 5).

Some of the most important chemical fingerprints shared by the two main lineages are: a moderate silica range (spanning ca. 10 wt%), with abundant more mafic granites (CI > 10; SiO₂ < 68 wt%); similar and nearly constant Na₂O (3.6 ± 0.2 wt%) and K₂O (4–5 wt%); moderate to high Sr (mostly in

TABLE I
Major and trace-element composition of granites and enclaves from the Piedade pluton.

Sample	MBmg (*samples with white K-feldspar megacrystals)									
	PD490E*	PD16	PD419	PD379	PD761	PD404	PD462	PD17C*	PD495B	PD852*
SiO ₂	64.03	64.68	64.81	65.08	65.29	65.44	66.34	66.81	67.24	67.76
TiO ₂	0.79	0.84	0.98	0.80	0.57	0.74	0.70	0.71	0.74	0.59
Al ₂ O ₃	16.47	16.09	15.85	16.15	15.79	15.91	15.60	16.06	15.23	15.68
Fe ₂ O ₃	4.76	4.61	5.15	3.90	4.31	4.13	3.95	4.37	4.21	3.54
MnO	0.05	0.07	0.07	0.05	0.06	0.07	0.05	0.05	0.06	0.04
MgO	1.43	1.44	1.84	1.07	1.26	1.27	1.23	1.29	1.36	1.17
CaO	2.73	2.59	2.85	2.37	2.29	2.59	2.49	2.33	2.68	2.30
Na ₂ O	3.47	3.52	3.73	3.07	3.43	3.51	3.46	3.46	3.65	3.47
K ₂ O	4.57	4.81	3.44	6.29	4.77	4.40	4.78	4.22	4.01	4.24
P ₂ O ₅	0.44	0.35	0.35	0.71	0.31	0.39	0.26	0.14	0.36	0.09
LOI	0.72	–	–	0.79	0.52	0.78	0.70	–	–	0.69
Total	99.46	99.00	99.07	100.28	98.60	99.23	99.56	99.44	99.54	99.57
Ni	< 20	–	10.47	–	–	–	6.34	< 20	–	–
Cr	–	36.4	18.78	11.4	–	–	15.57	17.1	–	–
Sc	–	5.4	5.72	3.6	–	–	5.3	6.4	–	–
V	54	68	81	61	56	73	53	44	49	48
Rb	204	180	193	217	–	184	–	179	–	–
Cs	5.3	4.6	4.14	3.5	–	–	2.43	4.4	–	–
Ba	1500	1530	1120	2104	1323	1297	1501	1250	1210	929
Sr	648	640	610	724	492	580	624	599	611	408
Zn	98	88	114	–	–	–	–	91	–	–
Ta	1.28	2.6	1.32	2.1	–	–	0.64	1.1	–	–
Nb	17.0	–	14.12	–	–	–	11.12	14.7	–	–
Co	16	–	10.48	–	–	–	6.48	8	–	–
Hf	7.6	6.3	7.67	8.1	–	–	7.33	7.6	–	–
Zr	311	210	262	363	239	320	256	301	267	201
Y	45.2	< 5	9.43	< 5	21	14	6.52	13.2	11	23
Pb	55	–	15.16	–	–	–	25.13	55	–	–
Th	17.8	10.5	14.1	5.3	–	–	12.53	28.2	–	–
U	2.31	2.0	1.6	2.7	–	–	0.88	3.0	–	–
W	< 0.5	–	1.00	–	–	–	1.83	< 0.5	–	–
Sn	2	–	3.27	–	–	–	4.02	2.0	–	–
La	80.6	81.3	96.66	68.7	48	86	59.86	89.3	81	94
Ce	135	151	178.86	134	–	–	109.24	158	–	–
Pr	15.7	–	18.21	–	–	–	11.28	17.9	–	–
Nd	56.0	45	63.52	44	–	–	39.15	60.7	–	–
Sm	8.68	6.14	10.09	6.90	–	–	5.98	9.46	–	–
Eu	1.98	1.51	1.97	1.80	–	–	1.46	1.67	–	–
Gd	7.50	–	5.78	–	–	–	3.59	6.36	–	–
Tb	1.22	< 0.5	0.77	< 0.5	–	–	0.47	0.83	–	–
Dy	6.65	–	2.94	–	–	–	1.87	3.30	–	–
Ho	1.30	–	0.37	–	–	–	0.25	0.46	–	–
Er	3.20	–	0.92	–	–	–	0.81	1.04	–	–
Tm	0.40	–	–	–	–	–	–	0.11	–	–
Yb	1.94	0.71	0.76	0.74	–	–	0.61	0.59	–	–
Lu	0.26	0.10	0.11	0.11	–	–	0.09	0.08	–	–
A/CNK	1.05	1.02	1.05	1.00	1.05	1.04	1.01	1.11	1.00	1.08
A/NK	1.55	1.46	1.61	1.36	1.46	1.51	1.44	1.57	1.47	1.52
Mg#	37.30	38.22	41.44	35.21	36.67	37.85	38.15	36.89	39.02	39.56
La _N /Yb _N	28.01	76.92	85.75	62.86	–	–	66.16	102.04	–	–
Eu/Eu*	0.75	–	0.79	–	–	–	0.96	0.66	–	–

TABLE I (continuation)

MBmg (*samples with white K-feldspar megacrystals)									
Sample	PD418	PD71	PD134	PD410	PD1152F	PD490B	PD1152E	PD240C*	PD406
SiO ₂	67.91	68.35	68.89	68.98	69.29	69.42	69.73	69.83	71.81
TiO ₂	0.62	0.61	0.58	0.63	0.57	0.43	0.56	0.49	0.56
Al ₂ O ₃	15.38	15.31	15.62	15.56	14.62	15.42	14.73	15.59	14.76
Fe ₂ O ₃	3.36	3.38	3.25	3.27	3.02	2.40	3.15	2.97	2.62
MnO	0.05	0.06	0.07	0.05	0.06	0.04	0.05	0.04	0.04
MgO	0.99	1.08	1.07	1.08	0.91	0.68	0.96	0.96	0.86
CaO	2.01	2.31	1.91	2.15	2.08	1.98	2.11	2.21	2.00
Na ₂ O	3.53	3.72	3.73	3.61	3.70	4.49	3.61	3.43	3.69
K ₂ O	4.76	4.52	5.18	4.45	4.16	4.31	4.33	4.67	4.53
P ₂ O ₅	0.25	0.21	0.21	0.14	0.20	0.17	0.22	0.16	0.19
LOI	0.66	–	–	–	–	0.58	–	0.73	–
Total	99.52	99.55	100.51	99.92	98.61	99.92	99.45	101.08	101.06
Ni	–	–	12.06	< 20	–	–	–	5.95	< 20
Cr	–	–	23.30	12.6	–	–	–	11.13	< 20
Sc	–	–	5.41	4.0	–	–	–	5.07	–
V	40	28	20	34	35	26	58	47	34
Rb	–	210	244	186	–	–	–	169	157
Cs	–	–	5.49	6.3	–	–	–	3.80	3.4
Ba	1263	1225	1133	1240	–	1362	953	991	1120
Sr	589	569	499	605	455	731	449	416	640
Zn	–	–	–	73	–	–	–	–	50
Ta	–	–	1.14	1.29	–	–	–	–	0.47
Nb	–	–	17.19	9.7	–	–	–	10.71	8.6
Co	–	–	5.66	6	–	–	–	5.37	4
Hf	–	–	8.27	6.7	–	–	–	4.77	5.7
Zr	249	–	292	276	206	168	205	198	217
Y	10	< 5	10.23	7.1	< 5	< 5	< 5	18.48	86.3
Pb	–	–	33.62	64	–	–	–	39.36	72
Th	–	–	23.92	13.1	–	–	–	21.84	17.0
U	–	–	2.01	3.54	–	–	–	3.50	2.08
W	–	–	0.33	–	–	–	–	0.56	< 0.5
Sn	–	–	3.76	4	–	–	–	2.34	4
La	72	69	108.51	81.2	87	65	90	60.72	73.7
Ce	–	–	174.47	140	–	–	–	109.13	92.4
Pr	–	–	18.21	15.3	–	–	–	12.43	13.9
Nd	–	–	56.80	50.9	–	–	–	44.00	57.0
Sm	–	–	7.08	6.47	–	–	–	8.08	9.69
Eu	–	–	1.01	1.42	–	–	–	1.55	3.11
Gd	–	–	3.60	3.64	–	–	–	5.62	11.8
Tb	–	–	0.50	0.36	–	–	–	0.92	1.59
Dy	–	–	2.25	1.44	–	–	–	4.29	8.73
Ho	–	–	0.33	0.24	–	–	–	0.69	1.84
Er	–	–	0.96	0.74	–	–	–	1.58	5.03
Tm	–	–	–	0.12	–	–	–	–	0.62
Yb	–	–	0.79	0.83	–	–	–	0.97	2.99
Lu	–	–	0.12	0.11	–	–	–	0.14	0.45
A/CNK	1.05	1.01	1.03	1.06	1.02	0.99	1.02	1.06	1.01
A/NK	1.40	1.39	1.33	1.45	1.38	1.28	1.39	1.46	1.35
Mg#	36.85	38.76	39.47	39.54	37.37	35.94	37.64	39.03	39.40
La _N /Yb _N	–	–	92.60	65.96	–	–	–	42.20	16.62
Eu/Eu*	–	–	0.61	0.89	–	–	–	0.70	0.89

TABLE I (continuation)

Sample	Bmg						
	PD420	PD1229	PD463	PD412	PD414	PD451	PD421B
SiO ₂	69.35	70.11	70.55	70.77	70.79	71.44	73.21
TiO ₂	0.46	0.44	0.40	0.42	0.41	0.39	0.29
Al ₂ O ₃	15.01	14.65	14.59	14.90	14.74	14.72	14.17
Fe ₂ O ₃	3.00	2.64	2.49	2.40	2.56	2.32	1.81
MnO	0.04	0.04	0.04	0.04	0.04	0.04	0.04
MgO	0.76	0.70	0.63	0.66	0.73	0.63	0.44
CaO	1.99	1.78	1.62	1.80	1.86	1.87	1.54
Na ₂ O	3.71	3.47	3.45	3.60	3.56	3.70	3.56
K ₂ O	4.65	5.04	5.07	4.80	4.48	4.73	4.70
P ₂ O ₅	0.18	0.15	0.15	0.17	0.15	0.13	0.05
LOI	0.51	–	–	–	0.46	0.54	0.54
Total	99.66	99.02	98.99	99.56	99.78	100.51	100.35
Ni	5.74	4.72	–	–	4.62	–	3.77
Cr	15.56	11.99	12.0	–	11.49	–	7.21
Sc	4.93	2.66	2.7	–	2.59	–	1.84
V	35	< 15	22	–	47	53	33
Rb	158	–	160	192	156	180	163
Cs	2.61	2.07	2.6	–	3.50	–	2.99
Ba	1007	1141	795	1027	1146	1023	807
Sr	462	512	310	465	532	477	358
Zn	–	–	58	178	–	–	–
Ta	0.15	0.37	< 0.5	–	0.18	–	0.62
Nb	5.23	4.71	–	–	5.27	–	6.38
Co	4.42	4.15	–	–	4.20	–	2.57
Hf	7.19	7.18	6.4	–	6.99	–	4.31
Zr	276	194	235	225	262	244	165
Y	4.33	11.54	< 5	–	4.55	–	4.50
Pb	41.11	27.64	–	–	31.15	–	35.75
Th	44.33	15.89	30.7	–	21.34	–	16.18
U	1.32	1.23	2.9	–	1.52	–	2.29
W	1.58	0.20	–	–	0.24	–	0.25
Sn	1.41	1.68	–	–	2.14	–	1.82
La	79.08	89.35	87.8	–	95.90	87	54.54
Ce	141.45	149.54	172	–	141.27	–	90.22
Pr	14.25	14.96	–	–	15.96	–	9.41
Nd	48.86	48.84	57	–	51.57	–	30.61
Sm	6.71	6.39	9.73	–	6.34	–	3.93
Eu	1.21	1.39	1.19	–	1.17	–	0.96
Gd	3.48	3.62	–	–	3.07	–	2.13
Tb	0.40	0.47	0.6	–	0.36	–	0.27
Dy	1.50	2.04	–	–	1.45	–	1.14
Ho	0.17	0.31	–	–	0.16	–	0.14
Er	0.62	0.93	–	–	0.51	–	0.44
Tm	–	–	–	–	–	–	–
Yb	0.41	0.73	0.59	–	0.43	–	0.37
Lu	0.07	0.12	0.05	–	0.07	–	0.06
A/CNK	1.02	1.02	1.03	1.04	1.05	1.01	1.03
A/NK	1.35	1.31	1.31	1.34	1.38	1.31	1.29
Mg#	33.41	34.43	33.38	35.26	36.09	34.97	32.50
La _N /Yb _N	130.00	82.52	100.60	–	150.40	–	99.38
Eu/Eu*	0.77	0.88	–	–	0.81	–	1.01

TABLE I (continuation)

Sample	BmgT							
	PD18A	PD481A	PD438	PD474B	PD64	PD1021	PD1037	PD439
SiO ₂	64.65	67.79	68.02	69.20	69.94	70.37	70.76	73.30
TiO ₂	1.00	0.66	0.65	0.61	0.55	0.61	0.46	0.25
Al ₂ O ₃	15.20	14.83	15.01	14.54	15.24	15.26	14.72	13.64
Fe ₂ O ₃	4.31	3.35	3.34	3.24	3.07	3.20	2.42	1.94
MnO	0.09	0.07	0.05	0.07	0.05	0.07	0.05	0.04
MgO	1.64	1.50	1.44	1.32	1.25	1.28	1.00	0.73
CaO	2.72	2.60	2.15	2.14	1.94	2.06	1.79	1.65
Na ₂ O	3.71	3.60	3.71	3.65	3.70	3.58	3.42	3.48
K ₂ O	4.47	4.36	4.94	4.75	4.92	5.08	5.16	4.06
P ₂ O ₅	0.48	0.27	0.28	0.28	0.24	0.21	0.20	0.13
LOI	0.61	0.56	–	–	–	–	–	0.47
Total	98.88	99.59	99.59	99.8	100.9	101.72	99.98	99.69
Ni	15.93	–	18.14	12.91	–	–	–	11.11
Cr	33.25	34.8	37.12	35.37	–	–	–	23.19
Sc	4.71	5.4	2.89	4.99	–	–	–	1.90
V	100	57	50	< 15	< 15	< 15	< 15	35
Rb	178	173	176	242	215	242	240	148
Cs	7.48	5.1	4.27	7.96	–	–	–	2.69
Ba	1438	1388	1535	1110	1361	1261	1103	862
Sr	839	768	675	500	602	545	462	438
Zn	–	–	75	91	–	–	–	–
Ta	2.12	< 0.5	1.99	2.08	–	–	–	0.35
Nb	18.59	–	17.63	19.20	–	–	–	4.59
Co	9.60	–	7.97	5.60	–	–	–	3.65
Hf	6.44	5.1	6.76	5.71	–	–	–	4.32
Zr	288	238	235	198	–	231	170	165
Y	17.71	12	412.10	20.65	45	8	9	< 5
Pb	19.34	–	30.83	27.09	–	–	–	25.80
Th	11.86	15.2	14.55	16.85	–	–	–	4.09
U	3.89	4.1	3.00	3.73	–	–	–	1.11
W	0.37	–	0.33	0.34	–	–	–	0.18
Sn	4.25	–	3.13	6.10	–	–	–	1.84
La	93.31	89.2	203.85	64.86	66	58	89	22.50
Ce	160.49	164	143.91	126.28	–	–	–	38.93
Pr	18.36	–	39.68	13.66	–	–	–	4.21
Nd	65.02	56	177.04	48.29	–	–	–	14.19
Sm	10.34	8.29	33.64	8.32	–	–	–	2.25
Eu	2.15	1.62	8.52	1.40	–	–	–	0.77
Gd	6.03	–	43.47	5.11	–	–	–	1.59
Tb	0.87	< 0.5	6.92	0.83	–	–	–	0.22
Dy	3.92	–	39.17	4.03	–	–	–	1.09
Ho	0.62	–	9.75	0.70	–	–	–	0.17
Er	1.58	–	25.67	1.98	–	–	–	0.47
Tm	–	–	–	–	–	–	–	–
Yb	1.28	1.00	17.19	1.62	–	–	–	0.41
Lu	0.19	0.12	2.52	0.24	–	–	–	0.07
A/CNK	0.96	0.96	0.98	0.97	1.02	1.01	1.02	1.04
A/NK	1.39	1.39	1.31	1.30	1.34	1.34	1.31	1.35
Mg#	42.97	47.00	46.06	44.65	44.64	44.20	45.01	42.70
La _N /Yb _N	49.15	60.00	8.00	26.99	–	–	–	37.00
Eu/Eu*	0.83	–	0.68	0.66	–	–	–	1.24

TABLE I (continuation)

Sample	Enclaves BmgT			Enclaves MBmg				granitoid lenses			
	PD481B	PD1205B	PD474A	PD1155B	PD490F	PD1155C	PD17D	PD1514	PD490A	PD415B	PD1152
SiO ₂	56.60	57.70	59.17	62.36	63.22	64.64	65.74	60.94	62.85	63.16	66.46
TiO ₂	1.70	1.84	1.59	1.38	1.34	1.21	1.01	1.52	0.88	0.63	0.46
Al ₂ O ₃	15.64	15.63	15.26	15.46	15.56	15.63	15.16	15.58	16.88	15.83	16.34
Fe ₂ O ₃	7.56	6.59	6.62	6.49	6.91	5.45	5.81	5.39	5.93	5.99	3.77
MnO	0.15	0.09	0.13	0.13	0.07	0.09	0.06	0.07	0.07	0.12	0.09
MgO	3.83	3.39	3.47	2.55	2.33	1.80	1.71	2.28	1.49	1.91	1.28
CaO	4.03	4.70	3.57	3.34	3.10	3.40	2.93	3.65	2.82	3.64	3.07
Na ₂ O	3.51	3.66	4.37	4.26	3.50	4.52	3.83	3.96	3.69	4.06	3.74
K ₂ O	4.25	3.71	3.19	2.37	2.71	1.82	2.26	4.49	4.78	3.73	4.12
P ₂ O ₅	0.75	0.75	0.58	0.57	0.38	0.38	0.33	0.63	0.39	0.44	0.21
LOI	1.05	1.72	0.91	1.09	0.86	0.79	0.96	–	0.80	–	–
Total	99.07	99.78	98.86	100.00	99.98	99.73	99.80	98.51	100.58	99.51	99.54
Ni	–	48.17	–	25	–	–	< 20	21.63	–	7.96	6.02
Cr	117.0	148.55	102.0	30	–	–	36	49.22	–	16.04	22.24
Sc	17.7	10.63	12.8	84	–	–	–	8.42	–	11.62	6.14
V	150	126	147	102	118	83	64	70	70	70	18
Rb	263	–	317	234	–	–	173	–	–	–	–
Cs	10.9	3.05	15.9	5.2	–	–	5.4	3.28	–	2.05	2.05
Ba	1186	1927	453	322	464	186	355	2565	1410	1529	1569
Sr	690	1196	522	404	467	441	458	1182	586	913	797
Zn	–	–	–	138	–	–	111	–	–	–	–
Ta	2.2	1.19	2.7	1.17	–	–	1.15	1.29	–	0.83	1.16
Nb	–	16.74	–	15.5	–	–	14.8	16.96	–	12.18	12.74
Co	–	19.10	–	–	–	–	11	14.98	–	11.21	7.51
Hf	8.1	6.64	5.9	6.4	–	–	4.8	6.35	–	5.27	4.88
Zr	383	214	255	254	217	239	214	225	285	184	165
Y	30	17	43	46.7	17	22	20.9	17.78	18	20.68	21.30
Pb	–	18.53	–	29	–	–	36	20.25	–	23.76	21.29
Th	12.8	10.82	12.4	11.6	–	–	8.19	11.34	–	10.00	11.60
U	5.0	2.61	11.0	1.87	–	–	1.79	2.27	–	1.73	1.57
W	–	0.89	–	< 0.5	–	–	< 0.5	0.20	–	0.16	0.09
Sn	–	2.72	–	7	–	–	2	2.95	–	1.87	2.34
La	103.0	77.48	142.0	98.4	45	55	41.6	91.98	103	54.51	66.18
Ce	268	154.90	273	158	–	–	75.4	189.86	–	97.54	106.18
Pr	–	17.30	–	23.2	–	–	8.81	20.42	–	11.72	12.05
Nd	107	65.22	132	89.1	–	–	31.8	74.26	–	44.90	42.66
Sm	17.00	10.79	20.50	15.7	–	–	5.85	11.62	–	8.44	6.91
Eu	3.56	2.77	4.49	2.21	–	–	1.27	2.92	–	2.24	1.83
Gd	–	6.44	–	11.8	–	–	4.74	6.78	–	5.70	4.75
Tb	2.1	0.94	1.8	1.50	–	–	0.78	0.98	–	0.88	0.76
Dy	–	4.10	–	6.89	–	–	4.06	4.26	–	4.20	3.73
Ho	–	0.63	–	1.17	–	–	0.68	0.63	–	0.75	0.69
Er	–	1.56	–	3.02	–	–	1.63	1.58	–	1.89	1.81
Tm	–	–	–	0.39	–	–	0.20	–	–	–	–
Yb	2.27	1.11	2.70	2.03	–	–	1.00	1.05	–	1.55	1.42
Lu	0.29	0.16	0.37	0.26	–	–	0.13	0.15	–	0.23	0.21
A/CNK	0.88	0.84	0.89	0.99	1.09	1.00	1.08	0.87	1.03	0.91	1.01
A/NK	1.51	1.56	1.43	1.61	1.79	1.66	1.73	1.37	1.50	1.48	1.54
Mg#	50.08	50.46	50.93	43.76	40.04	39.54	36.82	45.59	33.23	38.71	40.21
La _N /Yb _N	30.59	47.06	35.46	32.68	–	–	28.05	59.06	–	23.71	31.42
Eu/Eu*	–	1.02	–	0.50	–	–	0.74	1.01	–	0.99	0.98

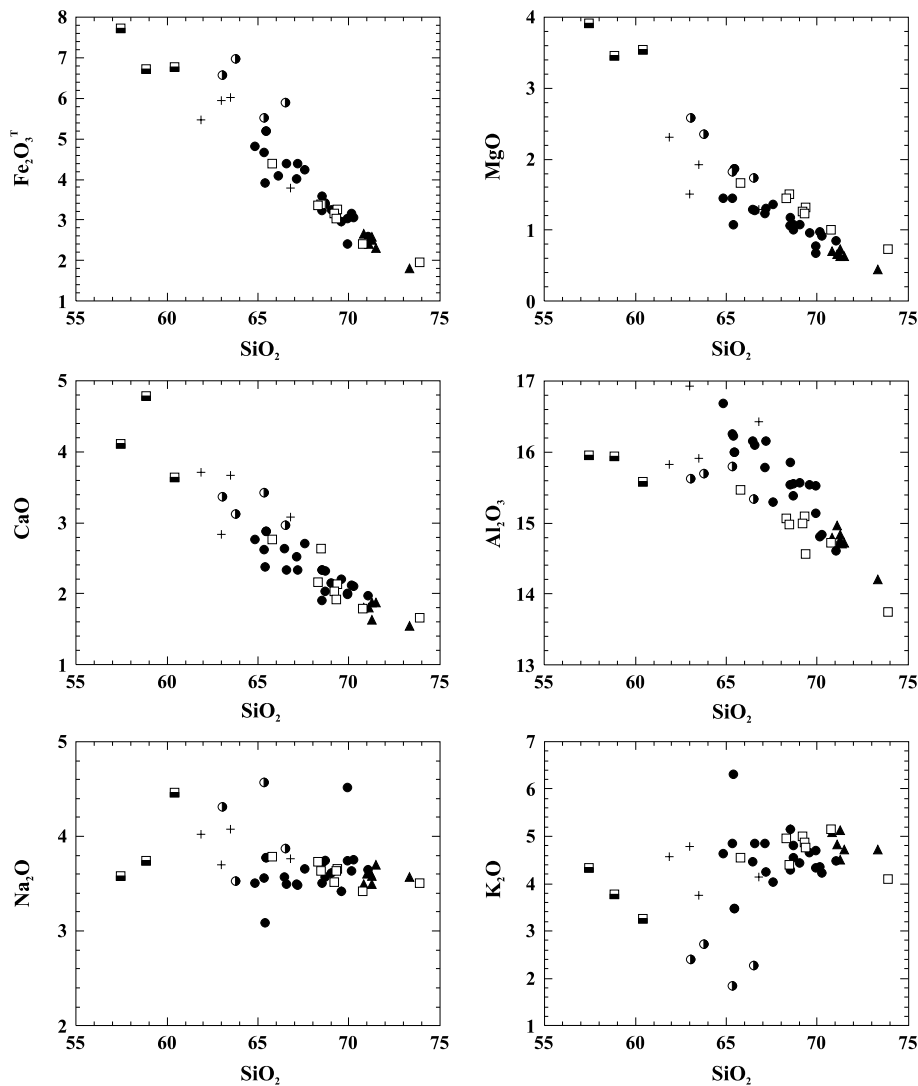


Fig. 5 – Major and trace-element variation diagrams using SiO_2 as a differentiation index for granites of the Piedade pluton. Symbols as in Figure 4.

the 400–800 ppm range) and Ba (800–1600 ppm), and low contents of HFS elements such as Zr, Nb and Ta. Such characteristics are comparable to those of high-K calc-alkaline suites from orogenic environments (e.g., Brown et al. 1984, Pearce et al. 1984).

The three biotite and titanite-rich enclaves from the BmgT unit are metaluminous, and in general seem to lie in the same trend defined by this unit projected to lower (57–60 wt%) SiO_2 values. Important scatter is however observed in LILE ele-

ments present in the biotite and feldspars (K, Na, Ba, Sr, Rb), which can be a result of open-system behavior, probably related to chemical exchange between enclaves and host granite.

The tonalite-granodiorite microgranular enclaves found in the northern portion of the MBmg unit are more SiO_2 -rich than the previous type, and show important chemical contrasts with their host, not following their evolutionary trend backwards (Figure 5). Although some systematic differences

are observed between the tonalite and granodiorite samples (e.g., the latter show higher K/Na, Ba, Fe, and are clearly peraluminous, while the first have $ASI \approx 1.0$), all these samples share important chemical characteristics not found in other rocks from the Piedade pluton, the more remarkable ones being their low Ba, Sr and K_2O contents.

Hornblende and epidote-bearing granodiorite enclaves and lenses found within the MBmg and Bmg units cover the same SiO_2 range as the previous type, but are metaluminous to slightly peraluminous, and show major and trace-element contents more similar to those of the associated granites. Lower TiO_2 and higher Sr, however, contrast these enclaves with the granite trends (Fig. 5).

RARE EARTH ELEMENTS

Chondrite-normalized rare-earth element patterns of granites from the Piedade pluton are presented in Figure 6. Common to all units is the moderate to strong fractionation ($La_N/Yb_N = 27-150$) and moderate to null negative Eu anomaly ($Eu/Eu^* = 0.6$ to 1.0). Typical samples from each of the main units are compared in Figure 6f, where the contrasts among them can be better observed.

The titanite-bearing BmgT granites have the least fractionated patterns ($La_N/Yb_N = 27-50$, Yb = 1.2–1.7 ppm (ca. 5–8 times chondrite) and Y = 12–21 ppm). The more felsic granites of the Bmg unit have the more fractionated patterns ($La_N/Yb_N = 83-150$), with very low Yb (0.4–0.6 ppm) and Y (4–7 ppm). The muscovite-bearing mafic granites (MBmg) show an intermediate REE behavior (Figure 6).

The least fractionated REE patterns of BmgT are mostly a reflection of the smaller medium to heavy rare-earth elements fractionation, as measured by the Gd_N/Yb_N ratio (2.1 to 3.8, compared to 3.5 to 7.0 in MBmg and Bmg samples with typical REE behavior). Their light to medium rare earths fractionation is similar to that shown by MBmg ($La_N/Sm_N \sim 5-6$). On the other hand, the strong fractionation typical of Bmg reflects both

light to medium and medium to heavy REE fractionation, and their high La_N/Sm_N (7–9) are only paralleled by two MBmg samples (PD134 and PD410).

Two samples with anomalous behavior are present in the BmgT unit. PD438 is anomalously rich in REE, in particular the HREE (and Y, see Table I). On the other hand, the silica-rich sample PD439 is depleted in REE and other trace-elements hosted in accessory minerals, such as Th and U (see also Figure 7); its pattern has a positive Eu anomaly ($Eu/Eu^* = 1.2$), probably reflecting the near-absence of REE-bearing accessory phases and the influence of feldspar as the main REE carrier in the rock. Both patterns could be produced by processes of depletion/accumulation of accessory minerals or feldspar in an as yet unknown (outcrop? chamber?) scale, and their REE behavior will not be further discussed here.

The REE patterns of the mica-rich enclaves present in BmgT mimic those of their host, but at higher contents (Figure 6a). On the other hand, the lens-shaped epidote and hornblende-bearing enclaves found in the other two units have REE patterns that are clearly less fractionated than those of their hosts, and resemble those of the least fractionated BmgT granites; note furthermore that sample PD1514, hosted in the more felsic Bmg unit, has a more fractionated REE pattern than the other two samples, which are hosted in MBmg.

SPIDERDIAGRAMS

Figure 7 shows patterns of incompatible element concentrations normalized to those of primitive mantle (Sun and McDonough 1989) for granites and enclaves from the Piedade pluton.

BmgT and Bmg differ in some important incompatible element ratios, with MBmg showing an intermediate behavior, in a similar way to what is observed for the REE. BmgT has higher average U, Nb and Ta, and lower Th and Nb/Ta as compared to Bmg (average Th/U ~ 4 , Nb/Ta ~ 9 in BmgT, and ~ 11 and 16 in Bmg). In the spiderdiagrams, these contrasts show up as deeper Ta troughs in Bmg, and mantle-normalized Th/U below unity in BmgT.

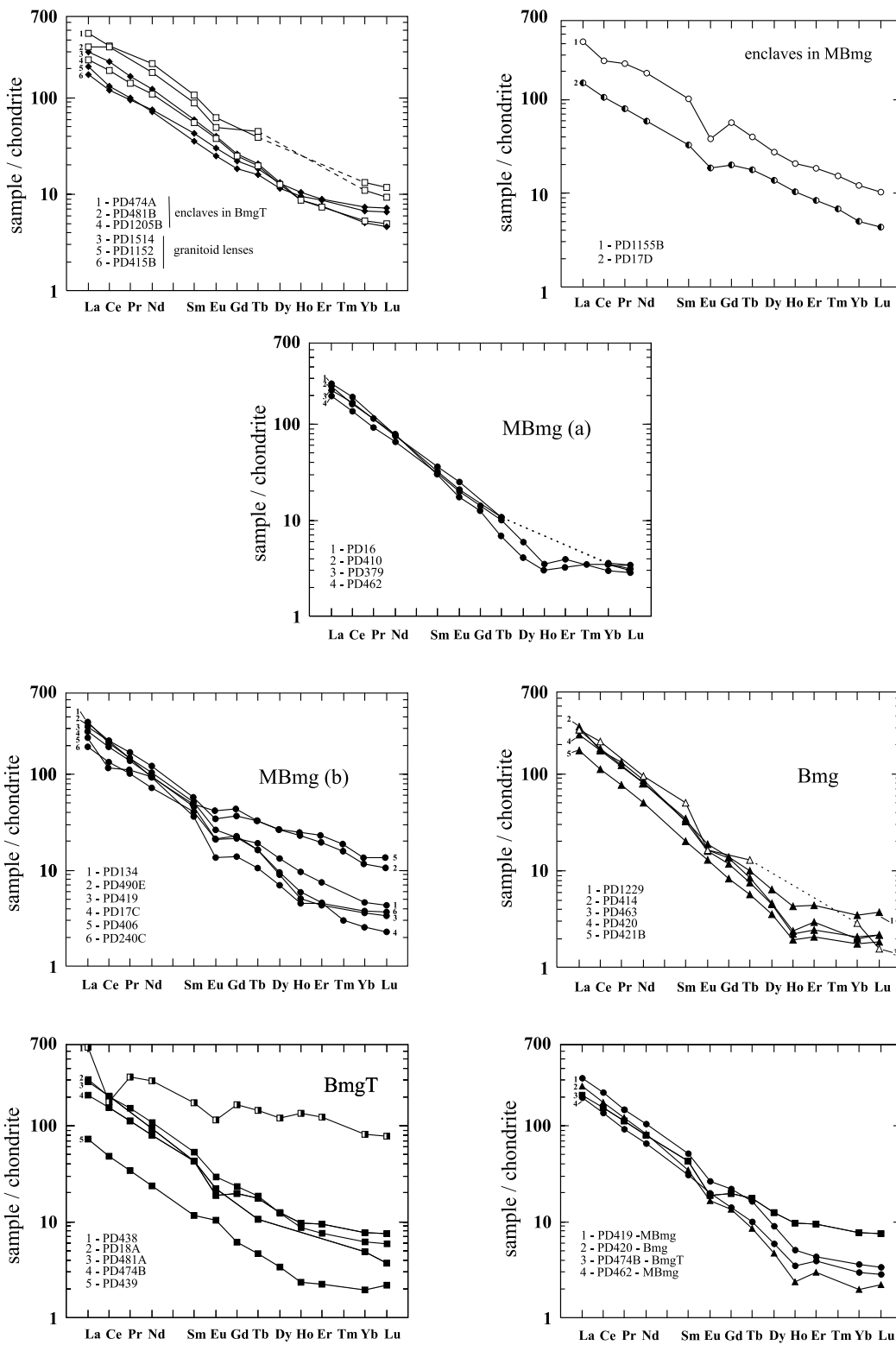


Fig. 6 – Chondrite-normalized (Boynton 1984) rare earth elements patterns for granites of the Piedade pluton.

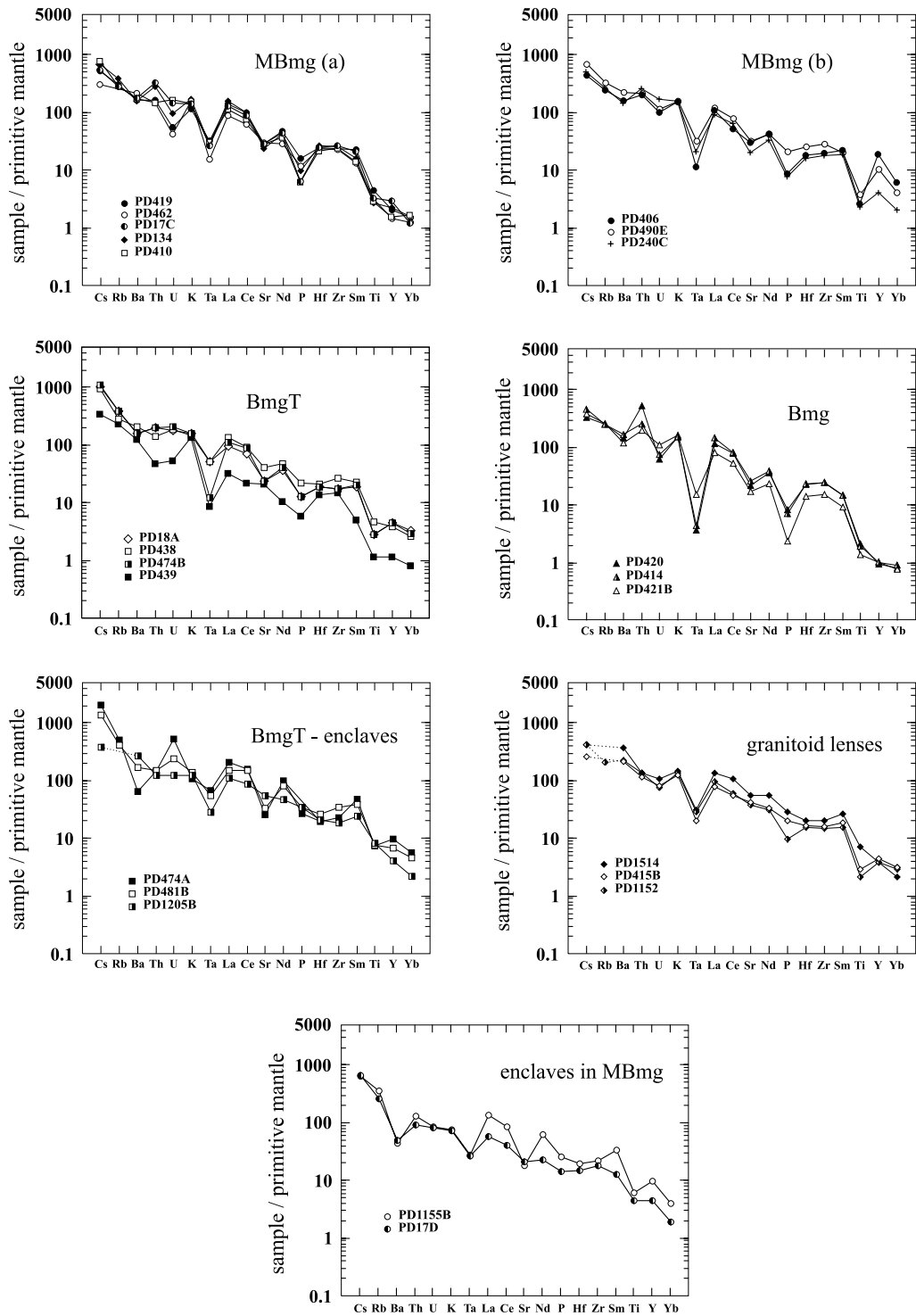


Fig. 7 – Behavior of the granites from the Piedade pluton in terms of Rb, Sr and Ba: (a) Rb x Sr; (b) Ba x Sr. Symbols as in Figure 3.

The BmgT enclaves are enriched in incompatible elements relative to their host.

Rb-Sr AND Sm-Nd ISOTOPE GEOCHEMISTRY

ANALYTICAL PROCEDURES

Rb-Sr and Sm-Nd isotope analyses were obtained by thermal ionization mass spectrometry (TIMS) at the Centro de Pesquisas Geocronológicas (Cepgeo), Instituto de Geociências, Universidade de São Paulo, using the procedures described by Sato et al. (1995). Three additional Sm-Nd analyses (samples PD420, PD462 and PD474b) were obtained at the Isotope Geochemistry Laboratory (IGL), University of Kansas, USA, also by TIMS; details of the analytical procedures at IGL are given in Janasi (2002).

THE RB-SR SYSTEM

Rb-Sr isotope analyses were done in a suite of BmgT samples spanning the whole compositional range of the unit in an attempt of obtaining an isochronic age. The resulting regression line yielded an age of 681 ± 21 Ma, with initial $^{87}\text{Sr}/^{86}\text{Sr}$ ratio of 0.7096 and $\text{MSWD} = 1.7$ (Figure 8a). This date is much older than the crystallization age of this unit, as determined by U-Pb zircon dating (604 ± 8 Ma; Janasi et al. 2001), and seems to reflect a contamination process, whereby the more fractionated samples (with lower Sr) have progressively higher $^{87}\text{Sr}/^{86}\text{Sr}_{600}$ (from 0.7102 to 0.7119, see Table II). Peraluminous granites from the MBmg and BMg units with Sr contents similar to those of the average BmgT granite have even higher $^{87}\text{Sr}/^{86}\text{Sr}_{600}$, around 0.713 (Table II; Figure 8a).

THE SM-ND SYSTEM

Sm-Nd isotope analyses were performed on seven representative samples of the main units of the Piedade pluton. The Sm-Nd T_{DM} model ages calculated using the DePaolo (1988) model vary from 1.7 to 2.1 Ga, within the range obtained for other granites from the Agudos Grandes batholith (Dantas et al. 2000, authors' unpublished data) and from other units of the Apiaí Fold Belt (K. Sato, unpublished

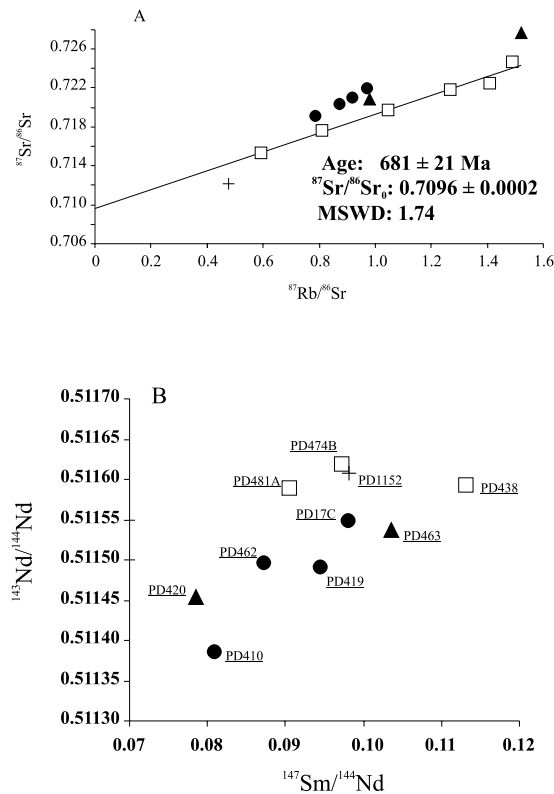


Fig. 8 – Rb-Sr and Sm-Nd isotope variation diagrams for granites of the Piedade pluton. In (a) the Rb-Sr isochron age obtained for the central unit (BmgT) is presented together with data from the other two main granite units; in (b) the Sm-Nd isotopic data for each analysed sample is presented; no isochrons were traced in view of the data scattering. Symbols as in Figure 3.

data, H. J. Prazeres Filho, unpublished data).

The ϵNd_{600} values are strongly negative, and vary from -12.3 in two samples of the BmgT unit to -15.6 in a muscovite-bearing sample from the border of the pluton (Table II). Such a range is well outside the uncertainties in the calculation of ϵNd_T and indicates that the samples cannot be related to each other by closed-system crystal fractionation processes. Therefore, either they derive from different sources or were affected by open-system processes such as contamination, magma mixing etc.

Some geographic zonation is suggested by the Nd isotope data, as the least negative ϵNd_{600} values are shown by two samples from the SW portion of

TABLE II

Rb-Sr and Sm-Nd radiogenic isotope composition of granites and enclaves from the Piedade pluton.

granite units	sample	Rb	Sr	$^{87}\text{Rb}/^{86}\text{Sr}$	error ^a	$^{87}\text{Sr}/^{86}\text{Sr}$	error ^b	$^{87}\text{Sr}/^{86}\text{Sr}_{(600)}$ ^c
HBgde	PD1152	134.0	812.1	0.478	0.0039	0.71211	0.00005	0.70802
MBmg	PD17C	198.7	634.7	0.907	0.0050	0.72184	0.00004	0.71408
	PD462	139.9	591.8	0.685	0.0070	0.71870	0.00003	0.71284
	PD419	192.7	641.4	0.870	0.0170	0.72043	0.00006	0.71298
	PD410	181.1	572.1	0.918	0.0120	0.72106	0.00001	0.71321
Bmg	PD420	155.2	457.6	0.983	0.030	0.72093	0.00008	0.71202
	PD463	167.2	319.2	1.519	0.006	0.72679	0.00013	0.71379
BmgT	PD481A	164.4	807.2	0.590	0.0084	0.71532	0.00007	0.71027
	PD474B	265.2	545.4	1.409	0.0400	0.72251	0.00007	0.71045
	PD438	184.4	660.1	0.809	0.0230	0.71765	0.00006	0.71073
	PD64	216.4	600.0	1.045	0.3000	0.71978	0.00009	0.71084
	PD1021	248.7	569.4	1.266	0.0360	0.72177	0.00008	0.71094
	PD1037	239.5	466.7	1.488	0.0420	0.72468	0.00008	0.71195

TABLE II (continuation)

granite units	sample	Sm	Nd	$^{147}\text{Sm} / ^{144}\text{Nd}$	error ^a	$^{143}\text{Nd} / ^{144}\text{Nd}$	error ^b	$\epsilon\text{Nd}_{600}^c$	TDM (Ga) ^d
HBgde	PD1152	7.325	45.147	0.0981	0.00040	0.5116080	0.000014	-12.5	1.85
MBmg	PD17C	8.398	51.893	0.0979	0.00040	0.5115500	0.000010	-13.7	1.91
	PD462	5.896	40.867	0.0872	0.00050	0.5114970	0.000012	-13.9	1.82
	PD419	10.992	70.377	0.0944	0.00030	0.5114910	0.000013	-14.5	1.93
	PD410	6.539	48.948	0.0808	0.00030	0.5113860	0.000031	-15.6	1.86
Bmg	PD420	6.509	50.122	0.0785	0.00050	0.5114520	0.000011	-14.1	1.76
	PD463	9.485	55.438	0.1035	0.00030	0.5115370	0.000011	-14.3	2.02
BmgT	PD481A	8.209	55.220	0.0905	0.00006	0.5115890	0.000022	-12.3	1.76
	PD474B	8.121	50.517	0.0972	0.00050	0.5116190	0.000012	-12.3	1.82
	PD438	35.654	190.679	0.1131	0.00040	0.5115930	0.000011	-14.0	2.12

^aMaximum error on Sm/Nd ratios is $\pm 0.5\%$, based on analytical uncertainties; maximum error on Rb/Sr ratios is $\pm 0.5\%$.

^bWithin-run precision on $^{143}\text{Nd}/^{144}\text{Nd}$ and $^{87}\text{Sr}/^{86}\text{Sr}$ expressed as 1 SE. ^cInitial values calculated at 600 Ma. ^dDepleted mantle model age, calculated according to DePaolo (1988).

the pluton, and the most negative ones are from its eastern border; samples from the three units having nearly the same intermediate value appear at the northern portion of the pluton (cf. figures 2, 9). This behavior could be a reflection of open-system processes in the site of magma crystallization, leading to scattering or homogenization of the isotope signatures.

THE $\epsilon_{\text{Nd}_T} \times {}^{87}\text{Sr}/{}^{86}\text{Sr}_T$ DIAGRAM

An $\epsilon_{\text{Nd}_T} \times {}^{87}\text{Sr}/{}^{86}\text{Sr}_T$ diagram grouping all samples for which data from both isotope systems are available shows a general tendency of higher ${}^{87}\text{Sr}/{}^{86}\text{Sr}_T$ and more negative ϵ_{Nd_T} in the muscovite-bearing MBmg unit as compared to the metaluminous BmgT unit (Figure 9). This behavior would be consistent with the first unit being a product of contamination of the latter by high Rb/Sr middle- to upper crust-derived material (see discussion below). Inter-unit variation is, however, also important, and there is much overlapping in the Nd isotope data (as previously pointed out, some samples from the three main units have the same $\epsilon_{\text{Nd}_{600}}$ values of -14). The magmatic epidote-bearing hornblende-biotite granodiorite sample is isotopically more primitive than its MBmg host, attesting to the lack of significant isotopic reequilibration within these small bodies. Moreover, its isotopic composition is the most primitive found in the Piedade pluton, and as such, more akin to that of the BmgT unit, suggesting some kind of link with the metaluminous granites.

PETROGENESIS

CONSTRAINTS FROM MAJOR-ELEMENT DATA

The Piedade pluton is dominated by relatively mafic-rich granites whose CI (~ 8 – 12), SiO_2 (65–70 wt%) and total (Fe+Mg+Ti) differ from the compositions typical of purely crust-derived melts (Patiño-Douce 1999). This is suggestive of an important contribution from mantle-derived basic magmas, what is reinforced by the common occurrence of dark enclaves of intermediate composition (down to 55–60 wt% SiO_2). The only granites that are

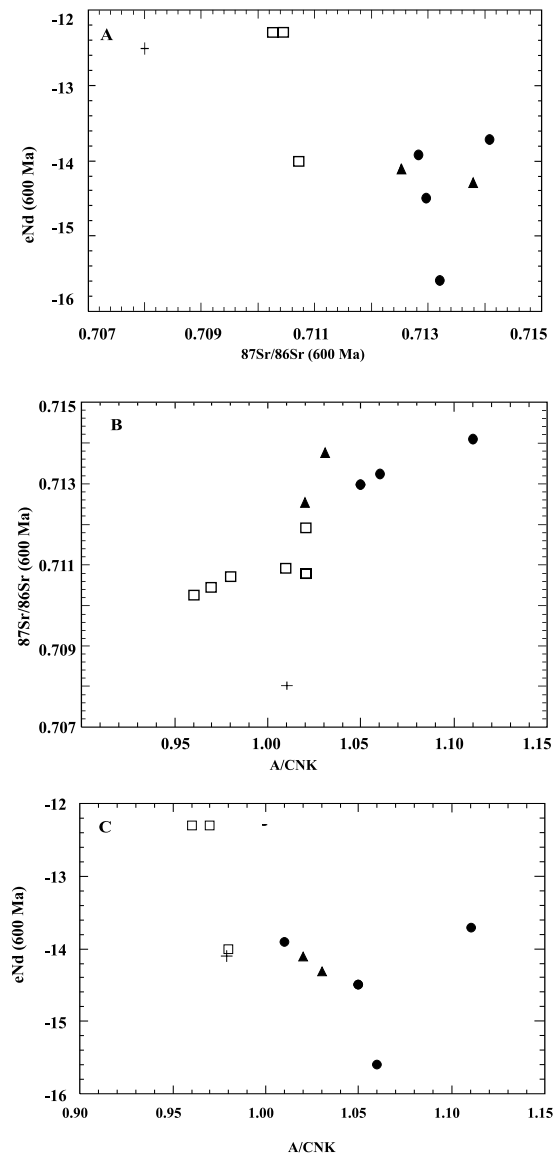


Fig. 9 – (a) $\epsilon_{\text{Nd}} (600 \text{ Ma})$ versus ${}^{87}\text{Sr}/{}^{86}\text{Sr} (600 \text{ Ma})$, (b) ${}^{87}\text{Sr}/{}^{86}\text{Sr} (600 \text{ Ma}) \times \text{ASI}$ (molecular $\text{Al}_2\text{O}_3 / \text{CaO} + \text{Na}_2\text{O} + \text{K}_2\text{O}$), (c) $\epsilon_{\text{Nd}} (600 \text{ Ma}) \times \text{ASI}$ for the Piedade granite. Symbols as in Figure 3.

felsic enough to correspond to pure crustal melts are those from Bmg unit, which appears as a ring between the central metaluminous (titanite-bearing) BmgT unit and the border peraluminous (muscovite and monazite-bearing) MBmg unit.

Two main contrasts in terms of major-element

geochemistry exist between the central and border units: the latter has, as indicated by mineralogy, higher Al_2O_3 at a similar SiO_2 and lower Mg# (averaging 38 as compared to 45 in BmgT).

Variations in the Mg# values of granite suites are usually good indications of fluctuations in the fO_2 (e.g. Debon and Lemmet 1999). The observed Mg# contrasts suggest that the peraluminous unit is more reduced as compared to the titanite-bearing metaluminous unit. This was confirmed by L. Martins (unpublished data) who showed that BmgT crystallized under extremely oxidizing conditions (NNO+2), based on biotite compositions and equilibria involving opaque minerals and titanite. Although it is on average more reduced, the redox state of the MBmg unit is strongly variable. The facies with white alkali feldspar is very reduced (\sim FMQ), and seems to have been subjected to post-magmatic oxidation that generated irregular transitions to pink varieties. It is unlikely, however, that the bulk of MBmg underwent such secondary processes. The strongly reduced facies has a small areal expression, being restricted to the outermost contact of the pluton. As it also shows some systematic chemical contrasts with the bulk of the unit, it could well be a product of local contamination with more reduced metasedimentary rocks that was later permeated by oxidizing fluids along fractures.

CONSTRAINTS FROM THE BEHAVIOR OF RB, SR AND BA

Ba, Rb and Sr are LILE present in major mineral phases such as feldspars and micas, and their behavior can be used to model the role of these minerals on the evolution of granite magmas. In the course of normal granite magma fractionation, Sr is usually the first to have a compatible behavior, as a result of plagioclase removal; it is commonly followed by Ba (taken up by K-feldspar), while Rb remains moderately incompatible up to the last more felsic differentiates, unless the magma is hydrous enough to stabilize biotite and/or muscovite early on. This is the case for samples from unit BmgT: Ba/Sr initially raises, then both elements decrease

together, and this ratio is kept nearly constant at 2.2–2.4 (Fig. 10b), which can be inferred as to be reflecting fractionation along the feldspar cotectics. Rb/Sr ratios rise continuously, and the most fractionated samples (anomalous sample PD439 excepted) reach \sim 240 ppm Rb (Fig. 10a).

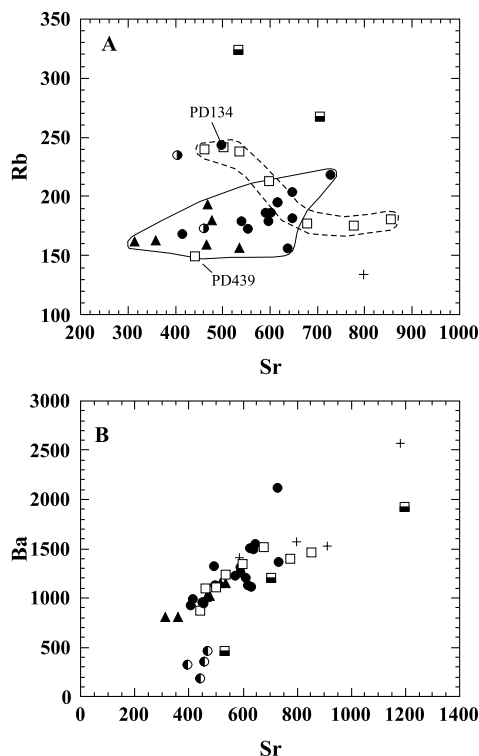


Fig. 10 – Behavior of the granites from the Piedade pluton in terms of Rb, Sr and Ba: (a) Rb x Sr; (b) Ba x Sr. Symbols as in Figure 3.

This tendency is not seen in the other two units. In particular, the felsic Bmg granites are Rb-poor (150–200 ppm), have the lowest Sr in the pluton, and clearly do not follow the BmgT fractionation trend (Fig. 10a). If Bmg derives from independent crust-derived magmas, the low Rb contents would be suggestive of significant residual biotite in the source (e.g., Harris and Inger 1992). Samples from the peraluminous MBmg unit have nearly the same Rb contents as those from the Bmg unit at higher Sr approaching those from BmgT (500–650 ppm; Fig. 10a).

The enclaves within the BmgT granites and the epidote-hornblende-bearing lenses tend to follow the behavior of unit BmgT, except for the very high Rb contents of the first, which is related to their high biotite content and could result from chemical exchange with the host granite. The tonalite-granodiorite enclaves within MBmg, however, are noticeably Ba-poor (< 500 ppm), in sharp contrast with the other rocks (Fig. 10b).

THE ORIGIN OF THE FRACTIONATED PINK GRANITES

Elemental and isotope geochemistry clearly demonstrates that the felsic Bmg granites are not the products of fractionation from the central metaluminous granites. Their relationship with the border MBmg unit is less clear. From field relations, it is interpreted that they could represent an inner more felsic unit, produced by “in situ” crystal fractionation. The major-element trends are consistent with those of MBmg, and both units seem to share a similar, more “evolved” Sr-Nd isotope signature.

The behavior of incompatible elements resident in accessory minerals, however, seems inconsistent with this simple relationship. In fact, Bmg are, on average, significantly poorer in U, Nb, Ta, Y and the HREE as compared to MBmg, even though the magmas that formed the latter unit should not be saturated in these elements.

The alternative hypothesis that Bmg derives from independent magmas and that the reasons for the observed chemical and isotope convergences with MBmg have to be sought on other causes must be considered. As pointed out earlier, Bmg is felsic enough that it could be the product of pure crustal melting, and the low Rb contents would suggest sources with residual biotite. Further constraints are given by the strongly fractionated REE patterns with absent to negligible negative Eu anomalies, arguing for a deep-seated (plagioclase-free, garnet-bearing) source. High Th/U is also consistent with sources in a deeper portion of the crust that was previously depleted in U. Low Nb and Ta could be a source feature (e.g., gneisses with calc-alkaline, “orogenic” signature) and/or these elements could

have been retained in phases residual or not involved in the melting reactions such as biotite, ilmenite or titanite.

In support to the hypothesis of an independent origin for Bmg is the remarkable geochemical similarity between these rocks and the late-orogenic pink equigranular granites that form a myriad of small bodies (not mappable at the scale of Fig. 2) intruding the metamorphic sequences in the Piedade region. However, they differ from all other felsic late-orogenic granites in the AGB by their slightly lower Ba/Sr ratios, a feature common to all Piedade granite units, and thought to be due to a “high-Sr” component typical of the regional high-K calc-alkaline granites (see R. J. Leite et al., unpublished data).

THE ORIGIN OF THE CENTRAL METALUMINOUS UNIT

The central BmgT unit has a relatively simple geochemical behavior and the internal variation can have resulted from simple crystal fractionation first involving the extraction of plagioclase (raising Ba/Sr) and then plagioclase + alkali feldspar (both Ba and Sr dropping). Local processes involving accessory phases appear to have been operative, responding for samples abnormally rich or poor in selected trace-elements (see above). On the other hand, the slightly variable $^{87}\text{Sr}/^{86}\text{Sr}$, which correlates positively with ASI, SiO_2 and $1/\text{Sr}$ in BmgT (e.g., Fig.9b), suggests that assimilation of more radiogenic material with higher Rb/Sr has accompanied crystal fractionation.

The predominant rock type in the metaluminous unit seems too mafic to be a pure crustal melt, and the abundance of intermediate enclaves with igneous textures can be a further indication that these rocks derive from hybrid melts which include a mantle-derived component (Barbarin 1999, Patiño-Douce 1999). This unit shares many geochemical features with the slightly older hornblende-biotite granites that form the bulk of the “syn-orogenic” plutons making up the Agudos Grandes batholith. Some remarkable differences such as their higher ASI (reflected in the absence of hornblende), higher Cs and U and lower $\epsilon\text{Nd}(t)$

are suggestive that BmgT carries a different component, probably metasedimentary material from upper crust with lesser residence time.

THE ORIGIN OF THE MAFIC-RICH PERALUMINOUS GRANITES

The mineralogical and chemical characteristics of the MBmg unit contrast them with mafic S-type granites from Australia and elsewhere (compare White and Chappell 1988, Chappell and White 1992). The lack of strongly peraluminous minerals such as cordierite and sillimanite is reflected in their ASI rarely exceeding 1.1 (Fig. 3b). Comparatively high Ca, Na and Sr contents as well as ASI and $^{87}\text{Sr}/^{86}\text{Sr}$ not significantly above those observed in nearby typically calc-alkaline granites are suggestive, instead, of a genetic link with the latter. The mafic-rich character of the MBmg unit is suggestive of a mafic to intermediate parent magma, thus possibly with a significant mantle-derived component. Several mechanisms are discussed in the literature whereby such a magma can assimilate metasedimentary material in its way up within the continental crust (cf. Ague and Brimhall 1988a, b, Patiño-Douce 1999, Castro et al. 1999).

Ague and Brimhall (1988a, b) identified significant variation in granites from the batholiths of California and admitted that their generation was a result of contamination of calc-alkaline magmas with crust-derived liquids and assimilation of wall-rocks. We notice that the chemistry and petrography of the Piedade MBmg variety with white alkali feldspar phenocrysts is similar to the I-SCR type (strongly contaminated and reduced I-type) in the western Sierra Nevada and Peninsular Range batholiths.

Subordinated peraluminous granites in the Mesozoic-Cenozoic Andean batholiths, predominantly composed of I-type granites, were denominated "S-like" (Avila-Salinas 1990, Suárez et al. 1990), supposing they are a result of I-type granite precursors that evolved by AFC, as suggested by initial $^{87}\text{Sr}/^{86}\text{Sr}$ ratios higher than those of nearby I-type granites.

Castro et al. (1999) suggested assimilation of crustal rocks by basaltic magmas as the mechanism responsible for the generation of the peraluminous granitoids in the Iberian massif, where significant variations are observed both in initial $^{87}\text{Sr}/^{86}\text{Sr}$ ratios (0.7074–0.7635) and ϵNd_T (+0.3 to –9.3). In their model, juvenile mantle magmas interacted with different crust material giving way to the variety of granites observed. Bea et al. (1999) also supposed that a close space-time association of mafic calc-alkaline, strongly peraluminous and alkaline granitic rocks in Iberia results from interaction between crustal and mantle-derived magmas.

MBmg forms the border of the Piedade pluton, and was locally injected as a series of thin sheets in country-rocks (migmatitic schists) that were possibly moderately hot. Although xenoliths are seen being assimilated in some outcrops, it appears that most of the contamination responsible for the peculiar composition of MBmg involved material with some chemical signatures unlike those expected from upper-crustal schists, such as high La/Yb and Th/U.

As pointed out before, it is in BmgT that such upper crust signature seems to be present, and the AFC process identified in that unit could involve such component. MBmg cannot be related to the same process, even though it appears to follow the same positive correlation between ASI and initial $^{87}\text{Sr}/^{86}\text{Sr}$ (Figure 9b): as shown in Fig. 8a, these granites are more mafic and have low Rb/Sr.

As discussed earlier (cf. Table I), MBmg has a distinctive behavior in terms of Mg# and key incompatible elements and ratios as U, Th/U, Nb, Ta, Nb/Ta, Y, Yb and La/Yb, which are on average intermediate between BmgT and Bmg. This is suggestive that Bmg could be the additional contaminant present in MBmg. However, MBmg shows the highest Al_2O_3 (and ASI, A/NK) and includes the more mafic rocks of the presently exposed section of the pluton, which is inconsistent with a simple mixing between BmgT and Bmg. If MBmg was formed by the interaction between crust-derived liquids similar to Bmg and a magma consanguineous with BmgT,

then the products of the latter that were involved in the process must have been more mafic than the rocks currently exposed at the core of the Piedade pluton.

ENCLAVES AND THEIR ROLE IN THE EVOLUTION OF THE PIEDADE PLUTON

Enclaves are recognized to bear important information on the genesis and evolution of their host granites (Didier and Barbarin 1991). The varied enclave typology seen in the Piedade granite reflects the operation of several mechanisms. The quartz-rich, muscovite-bearing enclaves found in some MBmg are chemically very distinctive, and may correspond to restite-rich cumulates. The metaluminous hornblende granodiorite with magmatic epidote present as lenses within MBmg is out of chemical and isotopic equilibrium with the host, and represents a different magma that was emplaced contemporaneously and had therefore potential to interact with it. This rock has some chemical and isotopic affinity with the core BmgT unit, and may correspond to injections of magmas related to the latter within the partly solidified border of the pluton. Fine-grained mafic microgranular enclaves are rarely found in the Piedade Granite, but an important enclave swarm within the more felsic Bmg unit suggests that contributions from coeval mafic magmas at the level of emplacement might have been important, and part of the magmatic enclaves such as the melagranites found in BmgT may be related to a mafic precursor.

CONCLUDING REMARKS

The ~ 600 Ma Piedade Granite is a zoned late-orogenic pluton made up of three contrasting units: porphyritic granites with relatively high color indices occur in the border (muscovite and monazite-bearing peraluminous granite-granodiorite MBmg, with CI = 8–15) and core (titanite and allanite-bearing biotite granite BmgT, with CI = 6–9), and are separated by a nearly continuous ring of more leucocratic, non-porphyritic pink granite (Bmg, with CI = 5–6).

It contrasts with slightly older (~ 610 Ma)

“syn-orogenic” porphyritic hornblende-biotite granites that make up most of the Agudos Grandes Batholith because of the predominance of peraluminous rock types and the occurrence of significant volumes of felsic (>70 wt% SiO₂) pink granites. Such slightly peraluminous felsic granites are the main or only components in other late-orogenic granites occurring to the west of Piedade, and also form countless small bodies intruding the regional metamorphic rocks.

Former workers have recognized the muscovite-bearing late-orogenic granites from the Piedade region as the products of crustal contamination of calc-alkaline magmas (Wernick et al. 1989, Janasi et al. 1990, Godoy et al. 1999). New elemental and isotope geochemical data here presented allow a better understanding of this process, in terms of the sources involved, the meaning of each of the main units, and the dynamics of the magma chamber.

The pink felsic granites are probably the products of crustal anatexis, and derive from deep-seated quartz-feldspatic sources within the garnet stability field (hence their strongly fractionated REE patterns without negative Eu anomalies). Geochemistry also constrain these sources to be poor in U and Nb-Ta and to have residual biotite (resulting in low Rb in the derived magmas).

The porphyritic granites are too mafic to be pure crustal melts, and must involve a mantle-derived basic component. The chemical variation within the core titanite-bearing BmgT unit points towards a simple crystal fractionation process coupled with some high Rb/Sr component assimilation (ACF) to respond for a slight increase in ⁸⁷Sr/⁸⁶Sr with differentiation. The more primitive rocks differ from the typical “syn-orogenic” high-K calc-alkaline granites in their higher A/CNK, less negative εNd(t) and higher contents of incompatible elements such as U and Cs. This may imply in a different crustal component, probably upper-crust metasedimentary material with lower crust residence time.

The border mafic-rich MBmg unit clearly owes

its peraluminous character to more strong crustal contamination. However, it is on average more mafic than BmgT and cannot be related to this unit through an ACF process. Assimilation of country rocks, although observed in a local scale, does not respond for the main chemical features of MBmg, which require a contaminant different from upper-crust schists, with high La/Yb and Th/U. Most of the trace-element and isotopic signature expected for the contaminant present in MBmg is found in Bmg (high La/Yb, Th/U, low Nb, Ta, Rb; also low Mg#). In terms of some important incompatible elements, MBmg has a behavior intermediate between Bmg and BmgT. The result of a simple mixing between magmas of average compositions equivalent to the two latter units would be more felsic and less Al-rich than MBmg; however, a more mafic magma consanguineous with BmgT could satisfy the requirements of such a model.

If a mixing process responds for some geochemical features of the Piedade Granite, it can be speculated whether it occurred at the site of emplacement or during magma ascent. As demonstrated in several recent studies, mixing between magmas of similar composition may be highly effective, sometimes leaving only scarce vestiges in geochemistry and/or accessory mineral zoning (Robinson and Miller 1999). Some of the features seen in the better-exposed northern portion of the Piedade pluton can be interpreted as the result of extensive interaction between originally more contrasted granitic magmas. In fact, south of the Piedade town both the BmgT and Bmg units disappear, and MBmg occurs in the area where they would have met each other (Fig. 2). There is also in this region some convergence between the three main units in terms of mineralogical, chemical and isotopic (e.g., $\epsilon\text{Nd}(t)$) characteristics. Swarms of pillowed mafic enclaves found locally within Bmg are another indication that the felsic magmas coexisted and partly mixed with more basic magmas at the site of emplacement.

A simplified model for the evolution of the Piedade Granite could be as follows. A first magma

pulse of mafic-rich calc-alkaline biotite monzodiorite to granodiorite magma was emplaced contemporaneously with felsic granite magma of composition equivalent to Bmg. As a result of efficient mixing the peraluminous MBmg unit was formed; the inward decrease in color index would reflect the increasing proportion of felsic granite melt in this direction. A second pulse of more fractionated calc-alkaline biotite granite melt intruded the center of the chamber and was mostly preserved from mixing except near the contacts with the previous units. Some synplutonic dikes with epidote and hornblende-bearing granodiorite only partly equilibrated with their host could be marginal manifestations related to this pulse.

ACKNOWLEDGMENTS

This research was supported by grants from Fundação de Amparo à Pesquisa do Estado de São Paulo (FAPESP, Proc. 97/0823-2 and 00/2509-8). R.J. Leite received Doctoral scholarships from Conselho Nacional de Desenvolvimento Científico e Tecnológico (CNPq) and Coordenação de Aperfeiçoamento de Pessoal de Nível Superior (CAPES). The authors thank Sandra Andrade for doing chemical analyses in part of the samples at the Instituto de Geociências, Universidade de São Paulo, and two anonymous referees for their careful reviews.

RESUMO

O Granito Piedade (~600 Ma) formou-se pouco tempo após a fase principal de magmatismo granítico no Batólito Agudos Grandes, Terreno Apiaí-Guaxupé, SE do Brasil. Suas principais unidades são: granitos porfíricos ricos em minerais máficos na borda (unidade MBmg, muscovita-biotita granodiorito-monzogranito peraluminoso) e núcleo (unidade BmgT, biotita monzogranito com titanita metaluminoso), e um biotita granito inequigranular félsico (unidade Bmg) aflorando entre eles. Bmg tem alto La_N/Yb_N (até 100), Th/U (>10) e baixo Rb, Nb e Ta, e pode ser um fundido crustal puro derivado de fontes profundas com granada e biotita residual. A unidade central BmgT deriva de magmas oxidados com alto Mg# (~45),

Ba e Sr, padrões de REE fracionados ($La_N/Yb_N = 45$), $^{87}Sr/^{86}Sr(t) \sim 0.710$, $\epsilon Nd(t) \sim -12$ a -14 , e é derivada de magmas cálcio-alcálicos potássicos levemente contaminados com rochas metassedimentares com assinatura de crosta superior (alto U, Cs, Ta). Os granitos peraluminosos ricos em minerais máficos mostram assinatura isotópica mais evoluída ($^{87}Sr/^{86}Sr(t) = 0.713-0.714$; $\epsilon Nd(t) = -14$ a -16), similar a Bmg, e Mg# e elementos-traço incompatíveis intermediários entre Bmg e BmgT. MBmg é interpretada como o produto de contaminação eficiente entre um magma rico em minerais máficos consanguíneo com BmgT e fundidos crustais puros similares a Bmg.

Palavras-chave: granito, cálcio-alcálico, peraluminoso, contaminação de magmas, geoquímica isotópica Sr-Nd.

REFERENCES

- AGUE JJ AND BRIMHALL GH. 1988a. Regional variations in bulk chemistry, mineralogy, and the compositions of mafic and accessory minerals in the batholiths of California. *Geol Soc Amer Bull* 100: 891–911.
- AGUE JJ AND BRIMHALL GH. 1988b. Magmatic arc asymmetry and distribution of anomalous plutonic belts in the batholiths of California: effects of assimilation, crustal thickness, and depth of crystallization. *Geol Soc Amer Bull* 100: 912–927.
- AVILA-SALINAS WA. 1990. Tin-bearing granites from the Cordillera Real, Bolivia; a petrological and geochemical review. In: KAY SM AND RAPELA CW (Eds), *Plutonism from Antarctica to Alaska*. *Geol Soc Amer Spec Paper* 241: 145–159.
- BARBARIN B. 1999. A review of the relationships between granitoid types, their origins and their geodynamic environments. *Lithos* 46: 605–626.
- BASEI MAS ET AL. 2003. Geochronology and isotope geochemistry of Votuverava and Perau Mesoproterozoic basins, southern Ribeira Belt, Brazil. In: *IV SOUTH AMERICAN SYMPOSIUM ON ISOTOPE GEOLOGY*, Salvador, BA, Brazil, p. 501–504.
- BEA F, MONTERO P AND MOLINA JF. 1999. Mafic precursors, peraluminous granitoids, and late lamprophyres in the Avila batholith: a model for the generation of Variscan batholiths in Iberia. *J Geol* 107: 399–419.
- BOYNTON WV. 1984. Geochemistry of the rare earth elements: meteorite studies. In: HENDERSON P (Ed), *Rare-earth element geochemistry*. Elsevier, p. 63–114.
- BROWN CG, THORPE RS AND WEBB PC. 1984. The geochemical characteristics of granitoids in contrasting arcs and comments on magma sources. *J Geol Soc London* 141: 413–426.
- CAMPANHA GAC AND SADOWSKI GR. 1999. Tectonics of the southern portion of the Ribeira Belt (Apiá Domain). *Precambr Res* 98: 31–51.
- CAMPOS NETO MC. 2000. Orogenic systems from Southwestern Gondwana: An approach to Brasiliiano-Pan-African cycle and orogenic collage in Southeastern Brazil. In: CORDANI UG, MILANI EJ, THOMAZ FILHO A AND CAMPOS DA (Eds), *Tectonic Evolution of South America*. 31st International Geological Congress, Rio de Janeiro, RJ, Brazil, p. 335–365.
- CASTRO A, PATIÑO-DOUCE AE, CORRETGE LG AND DE LA ROSA JD. 1999. Origin of peraluminous granites and granodiorites, Iberian massif, Spain: an experimental test of granite petrogenesis. *Contrib Mineral Petrol* 135: 255–276.
- CHAPPELL BW AND WHITE AJR. 1974. Two contrasting granite types. *Pacific Geol* 8: 173–174.
- CHAPPELL BW AND WHITE AJR. 1992. I- and S-type granites in the Lachlan Fold Belt. *Trans Royal Soc Edinb Earth Sci* 83: 1–26.
- COLLINS WJ AND HOBBS BE. 2001. What caused the Early Silurian change from mafic to silicic (S-type) magmatism in the eastern Lachlan Fold Belt? *J Austral Earth Sci* 48: 25–41.
- DANTAS EL, HACKSPACHER PC, FETTER AH, SATO K, PIMENTEL MM AND GODOY AM. 2000. Nd isotope systematics related to Proterozoic evolution of the central Ribeira belt in the state of São Paulo, SE Brazil. *Rev Bras Geocienc* 30: 140–143.
- DEBON F AND LEMMET M. 1999. Evolution of Mg/Fe ratios in Late Variscan Plutonic Rocks from the External Crystalline Massifs of the Alps (France, Italy, Switzerland). *J Petrol* 40: 1151–1185.
- DEPAOLO D J. 1988. Neodymium isotope geochemistry: an introduction. Springer Verlag, Berlin, Germany.

- DIDIER J AND BARBARIN B. 1991. Enclaves and Granite Petrology, Elsevier, Amsterdam.
- ELBURG MA. 1996. Genetic significance of multiple enclave types in a peraluminous ignimbrite suite, Lachlan Fold Belt, Australia. *J Petrol* 37: 1385–1408.
- GIMENEZ FILHO A, JANASI VA, CAMPANHA GAC, TEIXEIRA W AND TREVIZOLI JR LE. 2000. U-Pb dating and Rb-Sr isotope geochemistry of the eastern portion of the Três Córregos batholith, Ribeira Fold Belt, São Paulo. *Rev Bras Geocienc* 30: 45–50.
- GODOY AM, HACKSPACHER PC, OLIVEIRA MAF AND GOMES AB. 1999. Geoquímica dos Maciços Granitóides Ibiúna e Piedade na Folha Sorocaba. *Geociências* 18: 157–178.
- HARRIS NBW AND INGER S. 1992. Geochemical characteristics of pelite-derived granites. *Contrib Mineral Petrol* 110: 46–56.
- HASUI Y, PENALVA F AND HENNIES WT. 1969. Geologia do Grupo São Roque. In: XXIII CONGRESSO BRASILEIRO DE GEOLOGIA, Salvador, BA, Brasil, p. 101–134.
- HEILBRON M AND MACHADO N. 2003. Timing of terrane accretion in the Neoproterozoic–Eopaleozoic Ribeira orogen (SE Brazil). *Precamb Res* 125: 87–112.
- HEILBRON M, PEDROSA-SOARES AC, CAMPOS NETO MC, SILVA LC, TROUW RAJ AND JANASI VA. 2004. A Província Mantiqueira. In: MANTESSONETO V, BARTORELLI A, CARNEIRO CDR AND BRITO-NEVES BB (Coord), *Geologia do Continente Sul-Americano: Evolução da obra de Fernando Flávio Marques de Almeida*, São Paulo, Beca, p. 203–234.
- HILDRETH W AND MOORBATH S. 1988. Crustal contributions to arc magmatism in the Andes of Central Chile. *Contrib Mineral Petrol* 98: 455–489.
- JANASI VA. 2002. Elemental and Sr-Nd isotope geochemistry of two Neoproterozoic mangerite suites in SE Brazil: implications the origin of the mangerite-charnockite-granite series. *Precamb Res* 119: 301–327.
- JANASI VA, VASCONCELOS ACBC, VLACH SRF AND MOTIDOME MJ. 1990. Granitóides da região entre as cidades de São Paulo e Piedade (SP): faciologia e contexto tectônico. In: XXXVI CONGRESSO BRASILEIRO DE GEOLOGIA, Natal, RN, Brasil 4: 1925–1935.
- JANASI VA, ANDRADE S AND ULBRICH HHGJ. 1995. A correção do drift instrumental em ICP-AES com espectrômetro seqüencial e a análise de elementos maiores, menores e traços em rochas. *Bol IG-USP Sér Cient*, São Paulo 26: 45–58.
- JANASI VA, LEITE RJ AND VAN SCHMUS WR. 2001. U-Pb chronostratigraphy of the granitic magmatism in the Agudos Grandes Batholith (west of São Paulo, Brazil) – implications for the evolution of the Ribeira Belt. *J South Amer Earth Sci* 14: 363–376.
- JULIANI C, HACKSPACHER PC, DANTAS EL AND FETTER AH. 2000. The Mesoproterozoic volcano-sedimentary Serra do Itaberaba Group of the Central Ribeira Belt, São Paulo State, Brazil: implications for the age of the overlying São Roque Group. *Rev Brasil Geociênc* 30: 82–86.
- KEAY SM, COLLINS WJ AND MCCULLOCH MT. 1997. A three-component mixing model for granitoid genesis: Lachlan Fold Belt, eastern Australia. *Geology* 25: 307–310.
- PATIÑO-DOUCE A. 1999. What do experiments tell us about the relative contributions of crust and mantle to the origin of granitic magmas? In: CASTRO A, FERNÁNDEZ C AND VIGNERESSE JL (Eds), *Understanding granites: integrating new and classical techniques*. *Geol Soc London, Spec Publ* 168: 55–75.
- PEARCE JA, HARRIS NBW AND TINDLE AG. 1984. Trace-element discrimination diagrams for the tectonic interpretation of granitic rocks. *J Petrol* 25: 956–983.
- PIMENTEL MM, WHITEHOUSE MJ, VIANA MG, FUCK RA AND MACHADO N. 1997. The Mara Rosa arc in the Tocantins Province: further evidence for Neoproterozoic crustal accretion in central Brazil. *Precamb Res* 81: 229–310.
- PIUZANA P, PIMENTEL MM, FUCK RA AND ARMSTRONG R. 2003. SHRIMP U–Pb and Sm–Nd data for the Araxá Group and associated magmatic rocks: constraints for the age of sedimentation and geodynamic context of the southern Brasília Belt, central Brazil. *Precamb Res* 125: 139–160.
- PRAZERES FILHO HJ, HARARA OM, BASEI MAS, PASSARELLI CJ AND SIGA JR O. 2003. Litoquímica, geocronologia U-Pb e geologia isotópica (Sr-Nd-Pb) das rochas graníticas dos batólitos Cunhaporanga e Três Córregos na porção sul do Cinturão

- Ribeira, Estado do Paraná. *Geologia USP Sér Cient*, São Paulo 3: 51–70.
- ROBINSON DL AND MILLER CF. 1999. Record of magma chamber processes preserved in accessory mineral assemblages, Aztec Wash pluton, Nevada. *Amer Mineral* 84: 1346–1353.
- SATO K, TASSINARI CCG, KAWASHITA K AND PETRONILHO L. 1995. O método geocronológico Sm-Nd no IG/USP e suas aplicações. *An Acad Bras Cienc* 67: 315–336.
- SCHMIDT MW AND THOMPSON AB. 1996. Epidote in calc-alkaline magmas: An experimental study of stability, phase relationships, and the role of epidote in magmatic evolution. *Amer Mineral* 81: 462–474.
- SIAL AN, TOSELLI AJ, SAAVEDRA J, PARADA MA AND FERREIRA VP. 1999. Emplacement, petrological and magnetic susceptibility characteristics of diverse magmatic epidote-bearing granitoid rocks in Brazil, Argentina and Chile. *Lithos* 46: 367–392.
- SPANNER BG AND KRUHL JH. 2002. Syntectonic granites in thrust and strike-slip regimes: the history of the Carmo and Cindacta plutons (southeastern Brazil). *J South Amer Earth Sci* 15: 431–444.
- SUÁREZ M, NARANJO JA AND PUIG A. 1990. Mesozoic “S-like” granites of the central and southern Andes; a review. In: KAY SM AND RAPELA CW (Eds), *Plutonism from Antarctica to Alaska*: Boulder, Colorado. *Geol Soc Amer Spec Paper* 241: 27–32.
- SUN S-S AND MCDONOUGH WF. 1989. Chemical and isotopic systematic of oceanic basalts: implications for mantle compositions and processes. In: SAUNDERS AD AND NORRY MJ (Eds), *Magmatism in the ocean basins*. *Geol Soc London. Spec Publ* 42: 313–345.
- TASSINARI CCG, MUNHÁ JMU, RIBEIRO A AND CORREIA CT. 2001. Neoproterozoic oceans in the Ribeira Belt (southeastern Brazil): the Pirapora do Bom Jesus ophiolitic Complex. *Episodes* 24: 245–251.
- VLACH SRF, JANASI VA AND VASCONCELLOS ACBC. 1990. The Itu belt: associated calc-alkaline and aluminous A-type late Brasiliano granitoids in the States of São Paulo and Paraná, Southern Brazil. In: CONGRESSO BRASILEIRO DE GEOLOGIA 36, Natal, RN, Brazil 4: 1700–1711.
- WERNICK E, RIGO JR L, GALEMBECK TMB AND ARTUR AC. 1989. O Complexo Granitóide Ibiúna (SP): dados petrográficos e de tipologia de zircão. In: I SIMPÓSIO DE GEOLOGIA DO SUDESTE, Rio de Janeiro, *Boletim de Resumos*, p. 157–158.
- WHITE AJR AND CHAPPELL BW. 1988. Some supra-crustal (S-type) granites of the Lachlan Fold Belt. *Trans R Soc Edinb: Earth Sci* 79: 169–181.
- ZEN E-AN. 1986. Aluminum enrichment in silicate melts by fractional crystallization: some mineralogic and petrographic constraints. *J Petrol* 27: 1095–1117.